Saudi Pharmaceutical Journal 31 (2023) 101684

HOSTED BY

Contents lists available at ScienceDirect

Saudi Pharmaceutical Journal

journal homepage: www.sciencedirect.com

Original article

Design of semisynthetic derivatives of the Amaryllidaceae alkaloid ambelline and exploration of their *in vitro* cytotoxic activities

Aneta Ritomská [a], Darja Koutova [b], Jana Křoustková [a], Karel Královec [c], Darina Muthná [b], Jiří Kuneš [d], Lucie Nováková [e], Radim Havelek [b,*], Lucie Cahlíková [a,*]

[a] Department of Pharmacognosy and Pharmaceutical Botany, Faculty of Pharmacy, Charles University, Heyrovskeho 1203, Hradec Kralove 500 05, Czech Republic
[b] Department of Medical Biochemistry, Faculty of Medicine in Hradec Kralove, Charles University, Simkova 870, Hradec Kralove 500 03, Czech Republic
[c] Department of Biological and Biochemical Sciences, Faculty of Chemical Technology, University of Pardubice, Studentska 573, Pardubice 532 10, Czech Republic
[d] Department of Organic and Bioorganic Chemistry, Faculty of Pharmacy, Charles University, Heyrovskeho 1203, Hradec Kralove 500 05, Czech Republic
[e] Department of Analytical Chemistry, Faculty of Pharmacy, Charles University, Heyrovskeho 1203, Hradec Kralove 500 05, Czech Republic

ARTICLE INFO

Article history:
Received 21 March 2023
Accepted 17 June 2023
Available online 24 June 2023

Keywords:
Ambelline
Amaryllidaceae alkaloids
Antiproliferative activity
11-*O*-(4-Chloro-3-nitrobenzoyl)ambelline
Cytotoxicity
In vitro

ABSTRACT

Ambelline, an alkaloid from the Amaryllidaceae family with a crinane-type skeleton, has not yet demonstrated any outstanding biological activity. However, its analogues prepared by derivatization of the C-11 hydroxyl group show different interesting effects. Continuing our earlier work, twelve novel aromatic esters were developed (**10**, **14**, **16**, **17**, **22–25**, **30–33**) and studied, together with previously synthesized derivatives (**2–9**, **11–13**, **15**, **18–21**, **26–29**) in terms of their cytotoxic activity. The cytotoxic potential was determined on a panel of nine human cancer cell lines and one noncancerous cell line to characterize their biological activity spectrum. To describe and foresee the structure–activity relationship for further research, substances synthesized and described in our previous work were also included in this cytotoxicity study. The most significant activity was associated with analogues having methyl (**10**), methoxy (**14–17**), or ethoxy (**18**) substitution on the phenyl condensed to ambelline. However, the 4-chloro-3-nitrobenzoyl derivative (**32**) showed the most promising IC_{50} values, ranging from 0.6 ± 0.1 μM to 9.9 ± 0.2 μM. *In vitro* cytotoxicity studies indicated the most potent antiproliferative activity of **32** in a dose-dependent and time-dependent manner. Besides, **32** was found to be effective in decreasing viability and triggering apoptosis of MOLT-4 T-lymphoblastic leukemia cells.

© 2023 The Author(s). Published by Elsevier B.V. on behalf of King Saud University. This is an open access article under the CC BY-NC-ND license (http://creativecommons.org/licenses/by-nc-nd/4.0/).

1. Introduction

Cancer is the second leading cause of death worldwide, causing almost 10 million deaths in 2020. However, the incidence increased to 19.3 million new cases and continues to grow (Ferlay et al., 2021). The primary treatment consists of prescribed antineoplastic drugs, surgical removal of the tumour, radiotherapy, or a combination of these. Antineoplastic drugs are divided into two types – conventional chemotherapy and targeted therapy. Conventional chemotherapy remains the first-line treatment for many cancers, even though the biggest drawback of these antineoplastics is their high chemical reactivity, leading to increased toxicity and instability. Targeted therapy is also available, in which the mechanism of action is more specific and has reduced numbers of side effects (Guichard et al., 2017). The best-selling cancer drugs are either synthetic ones or monoclonal antibodies, but substances based on natural products fill roughly 60% of cancer treatment (Cragg and Pezzuto 2016). Some phytochemical substances persist as vital sources of new derivatives and potential drugs for cancer therapy due to their prominent effects on cancer cells along with acceptable toxicity in normal cells. The best examples used in clinical practice are vinca alkaloids, paclitaxel analogues, and podophyllotoxin analogues (Choudhari et al., 2020).

Abbreviations: CI, cell index; ECACC, European Collection of Authenticated Cell Cultures; PBS, phosphate-buffered saline; PI, propidium iodide; RTCA, real-time cell analysis; SD, standard deviation.

* Corresponding authors.
E-mail addresses: havelekr@lfhk.cuni.cz (R. Havelek), cahlikova@faf.cuni.cz (L. Cahlíková).

Peer review under responsibility of King Saud University. Production and hosting by Elsevier.

Production and hosting by Elsevier

https://doi.org/10.1016/j.jsps.2023.06.017
1319-0164/© 2023 The Author(s). Published by Elsevier B.V. on behalf of King Saud University.
This is an open access article under the CC BY-NC-ND license (http://creativecommons.org/licenses/by-nc-nd/4.0/).

Isoquinoline alkaloids from the Amaryllidaceae family are an important class of bioactive compounds. They have encouraged great interest in recent years due to their broad spectrum of pharmacological effects, such as antibacterial, antiviral, antifungal, antiparasitic, antimalarial, analgesic, neuroprotective, and potentially also antitumor activity (He et al., 2015; Habartova et al., 2016; Cahlikova et al., 2021). The antitumor properties were already known in the 4th century BCE and up to now, more than 600 Amaryllidaceae alkaloids of various structural types have been isolated. Among them, lycorine, narciclasine, and pancratistatin have the most promising cytotoxic activity at micromolar levels (Cao et al., 2013; Nair and van Staden 2014; Furst 2016; Youssef et al., 2022).

In the presented study, we developed a new series of ambelline derivatives to increase their cytotoxic activity. The main advantage of ambelline as a starting material for semi-synthesis is its relatively easy isolation from fresh bulbs of *Nerine bowdenii* (Amaryllidaceae), where it is the second major alkaloid after belladine. Ambelline is a colourless substance with lozenge-shaped crystals and belongs to the crinine structural type of Amaryllidaceae alkaloids. Ambelline as a pure substance has not been considered an interesting lead structure for future drug design due to the lack of any significant biological activity. However, its semi-synthetic derivatives showed promising cholinesterases inhibitory activity. From the entire spectrum of tested derivatives, eleven of them were described as selective inhibitors of human butyrylcholinesterase (*h*BuChE) (Marikova et al., 2020). The inspiration for the preparation of these derivatives lies in the structural similarity of ambelline with haemanthamine, which together with it belongs to the crinane type of Amaryllidaceae alkaloid. However, their tetrahydro-5,10b-ethanophenanthridine skeletons are essentially enantiomers that differ in the orientation of ethylene connecting N-5 and C-10b. The α-oriented bridge (projecting behind the plane of the paper) is characteristic of the haemanthamine type (α-crinane scaffold), and the opposite is the crinine type (β-crinane scaffold) (Ding et al., 2017). The nomenclature can be quite confusing, as some of the alkaloids are actually only enantiomers with different names (e.g. levorotatory crinine with a β-crinane scaffold, dextrorotatory vittatine with an α-crinane scaffold).

Regarding the biological effects of haemanthamine representing α-crinanes and ambelline representing β-crinanes (Fig. 1), they differ significantly. (Nair et al., 2013a, 2013b, 2013c; Nair and van Staden 2019). For example, the cytotoxicity of ambelline has been tested across different tumour cell lines with no significant results (Campbell et al., 1998; McNulty et al., 2007; Berkov et al., 2011; Luchetti et al., 2012; Hanh et al., 2018). On the other hand, haemanthamine has often been purposefully tested as an agent with considerable cytotoxic potential (Nair et al., 2013a, 2013b, 2013c; Doskocil et al., 2015; Havelek et al., 2017; Seifrtova et al., 2017; Pellegrino et al., 2018; Masi et al., 2022).

Many structure–activity relationship (SAR) studies have been performed using both natural compounds and their synthetic derivatives. The outputs of these studies, including intact partially saturated phenanthridine, the presence of a methylenedioxyphenyl moiety, and small electronegative substituents at C-11, were incorporated in our study. Surprisingly, active cytotoxic molecules were reported in both subgroups of the crinane skeleton. However, the orientation of the 5,10b-ethylene bridge affects the cytotoxic efficacy (Nair et al., 2013a, 2013b, 2013c; 2015). Thus, a comparison of the ambelline and haemanthamine analogues (Fig. 1) may advance the SAR regarding a wide range of biological activities, not just cytotoxicity.

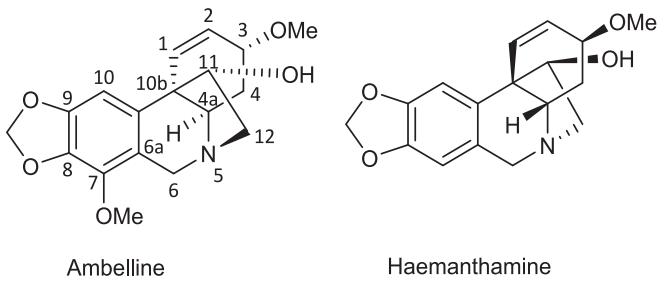

Fig. 1. Structure of ambelline and haemanthamine.

2. Material and methods

2.1. General experimental procedures

All solvents were treated by using standard techniques before use. All reagents and catalysts were purchased from Sigma Aldrich, Czech Republic, and used without purification. NMR spectra were recorded in $CDCl_3$ on a VNMR S500 (Varian) spectrometer operating at 500 MHz for proton nuclei and 125.7 MHz for carbon nuclei at ambient temperature. Chemical shifts were recorded as δ values in parts per million. The residual signal of $CDCl_3$ (δ 7.26 ppm) was applied as a reference for ^{1}H NMR spectra, and the central signal of the $CDCl_3$ signals (δ 77.0 ppm) was used as a reference for proton-decoupled ^{13}C NMR spectra. Coupling constants (*J*) are given in Hz. ESI-HRMS were obtained with a Waters Synapt G2-Si hybrid mass analyser of a quadrupole-time-of-flight (Q-TOF) type, coupled to a Waters Acquity I-Class UHPLC system. The EI-MS were obtained on an Agilent 7890A GC 5975 inert MSD operating in E.I. mode at 70 eV (Agilent Technologies, Santa Clara, CA, USA). A DB-5 column (30 m × 0.25 mm × 0.25 μm, Agilent Technologies, USA) was used. The temperature program was 100–180 °C at 15 °C/min, 1 min hold at 180 °C, and 180–300 °C at 5 °C /min and 5 min hold at 300 °C; detection range *m/z* 40–600. The injector temperature was 280 °C, and the carrier gas (helium) flow rate was 0.8 mL/min. A split ratio of 1:15 was used. TLC was carried out on Merck precoated silica gel 60 F254 plates. Compounds on the plate were observed under UV light (254 and 366 nm) and visualized by spraying with Dragendorff's reagent.

2.2. Isolation of ambelline (1)

Ambelline used for the preparation of this series of derivatives was obtained during the phytochemical study of *Nerine bowdenii* W. Watson (Vaneckova et al., 2016). High resolution mass spectrometry and NMR spectroscopy confirmed the purity of ambelline (≥98%).

2.3. Preparation of ambelline derivatives

The general procedure for the esterification of ambelline was described in detail in our previous work. Structural analyses (optical rotation, HRMS, NMR) of previously prepared derivatives (**2–9, 11–13,15,18–21,26–29**) can be found in the following literature (Marikova et al., 2020).

2.3.1. 11-O-(3,5-Dimethylbenzoyl)ambelline (10)

Yield 67 mg (94%); white powder; $[\alpha]_D^{24}$= +20.2 (*c* = 0.139; $CHCl_3$); ^{1}H NMR (500 MHz, $CDCl_3$) δ: 7.22 (2H, s), 7.12 (1H, s), 6.59 (1H, d, *J* = 10.0 Hz), 6.57 (1H, s), 6.08 (1H, dd, *J* = 10.0 Hz, *J* = 5.2 Hz), 5.86 (1H, d, *J* = 1.5 Hz), 5.80 (1H, d, *J* = 1.5 Hz), 5.33 (1H, dd, *J* = 8.0 Hz, *J* = 4.0 Hz), 4.37 (1H, d, *J* = 17.5 Hz), 4.00 (3H, s), 3.93 (1H, overlap, d, *J* = 17.5 Hz), 3.93–3.87 (2H, overlap, m), 3.53 (1H, ddd, *J* = 13.7 Hz, *J* = 4.0 Hz, *J* = 1.7 Hz), 3.37 (3H, s), 2.80 (1H, ddd, *J* = 14.2 Hz, *J* = 4.0 Hz, *J* = 1.7 Hz), 2.28 (6H, s), 2.21–2.16

(1H, m), 1.79 (1H, td, *J* = 13.7 Hz, *J* = 4.0 Hz); ^{13}C NMR (125.7 MHz, $CDCl_3$) δ: 166.4, 147.8, 140.6, 137.7, 134.5, 133.9, 133.8, 131.2, 129.7, 127.2, 126.6, 117.3, 100.5, 99.6, 87.3, 72.2, 63.0, 59.8, 59.1, 58.6, 56.5, 47.5, 28.7, 21.0; ESI-HRMS: *m*/*z* calcd for $C_{27}H_{30}NO_6^+$ $[M + H]^+$ 464.2068, found 464.2067.s.

2.3.2. 11-O-(2,4-Dimethoxybenzoyl)ambelline (14)

Yield 50 mg (67%); yellow powder; $[\alpha]_D^{24}$= +80.0 (*c* = 0.145; $CHCl_3$); ^{1}H NMR (500 MHz, $CDCl_3$) δ: 6.82 (2H, d, *J* = 2.4 Hz), 6.63–6.57 (3H, m), 6.09 (1H, dd, *J* = 10.1, *J* = 5.2 Hz), 5.84 (1H, d, *J* = 1.5 Hz), 5.79 (1H, d, *J* = 1.5 Hz), 5.33 (1H, dd, *J* = 8.0, *J* = 3.9 Hz), 4.37 (1H, d, *J* = 17.5 Hz), 3.99 (3H, s), 3.97–3.87 (3H, m), 3.76 (6H, s), 3.52 (1H, dd, *J* = 13.8, *J* = 3.9 Hz), 3.38 (3H, s), 2.80 (1H, ddd, *J* = 14.3, *J* = 3.9, *J* = 1.7 Hz), 2.23–2.16 (1H, m), 1.80 (1H, td, *J* = 13.8, *J* = 3.9 Hz); ^{13}C NMR (125.7 MHz, $CDCl_3$) δ: 166.0, 160.5, 147.8, 140.7, 133.9, 133.8, 131.6, 131.2, 126.8, 117.5, 106.7, 106.4, 100.5, 99.5, 87.9, 72.2, 63.1, 59.9, 59.1, 58.7, 56.6, 55.4, 47.2, 28.7; ESI-HRMS: *m*/*z* calcd for $C_{27}H_{30}NO_8^+$ $[M + H]^+$ 496.1966, found 496.1972.

2.3.3. 11-O-(3,5-Dimethoxybenzoyl)ambelline (16)

Yield 58 mg (75%); yellow powder; $[\alpha]_D^{24}$= +32.4 (*c* = 0.148; $CHCl_3$); ^{1}H NMR (500 MHz, $CDCl_3$) δ: 6.80 (2H, d, *J* = 2.5 Hz), 6.60–6.55 (3H, m), 6.07 (1H, dd, *J* = 10.3 Hz, *J* = 4.9 Hz), 5.81 (1H, d, *J* = 1.4 Hz), 5.77 (1H, d, *J* = 1.4 Hz), 5.31 (1H, dd, *J* = 7.8 Hz, *J* = 3.9 Hz), 4.35 (1H, d, *J* = 17.1 Hz), 3.99 (3H, s), 3.94–3.85 (3H, m), 3.73 (6H, s), 3.50 (1H, dd, *J* = 13.6 Hz, *J* = 3.9 Hz), 3.35 (3H, s), 2.82–2.75 (1H, m), 2.17 (1H, dd, *J* = 14.2 Hz, *J* = 3.9 Hz), 1.78 (1H, td, *J* = 13.6 Hz, *J* = 3.9 Hz); ^{13}C NMR (125.7 MHz, $CDCl_3$) δ: 165.9, 160.4, 147.7, 140.6, 133.9, 133.7, 131.6, 131.1, 126.7, 117.3, 106.6, 106.3, 100.4, 99.4, 87.8, 72.1, 63.0, 59.9, 59.1, 58.7, 56.5, 55.3, 47.2, 28.6; ESI-HRMS: *m*/*z* calcd for $C_{27}H_{30}NO_8^+$ $[M + H]^+$ 496.1966, found 496.1977.

2.3.4. 11-O-(3,4,5-Trimethoxybenzoyl)ambelline (17)

Yield 17 mg (36%); white powder; $[\alpha]_D^{24}$= +83.3 (*c* = 0.120; $CHCl_3$); ^{1}H NMR (500 MHz, $CDCl_3$) δ: 6.94 (2H, s), 6.62 (1H, s), 6.58 (1H, d, *J* = 10.0 Hz), 6.08 (1H, dd, *J* = 10.0 Hz, *J* = 5.1 Hz), 5.80 (2H, s), 5.31 (1H, dd, *J* = 7.9 Hz, *J* = 3.9 Hz), 4.36 (1H, d, *J* = 17.6 Hz), 3.98 (3H, s), 3.97–3.87 (3H, m), 3.86 (3H, s), 3.81 (6H, s), 3.49 (1H, dd, *J* = 13.8 Hz, *J* = 3.9 Hz), 3.37 (3H, s), 2.77 (1H, ddd, *J* = 14.2 Hz, *J* = 3.9 Hz, *J* = 1.4 Hz), 2.22–2.16 (1H, m), 1.80 (1H, td, *J* = 13.8 Hz, *J* = 3.9 Hz); ^{13}C NMR (125.7 MHz, $CDCl_3$) δ: 165.8, 152.7, 147.6, 142.1, 140.7, 134.1, 133.7, 131.0, 126.9, 124.7, 117.4, 106.5, 100.5, 99.4, 87.9, 72.2, 63.0, 60.8, 60.1, 59.1, 58.8, 56.6, 55.9, 47.0, 28.7; ESI-HRMS: *m*/*z* calcd for $C_{28}H_{32}NO_9^+$ $[M + H]^+$ 526.2072, found 526.2077.

2.3.5. 11-O-(3,5-Dinitrobenzoyl)ambelline (22)

Yield 60 mg (76%); yellow powder; $[\alpha]_D^{24}$= +137.1 (*c* = 0.105; $CHCl_3$); ^{1}H NMR (500 MHz, $CDCl_3$) δ: 9.16 (1H, bs), 8.67 (2H, bs), 6.54 (1H, d, *J* = 10.1), 6.51 (1H, s), 6.13 (1H, dd, *J* = 10.1 Hz, *J* = 5.2 Hz), 5.94–5.87 (2H, m), 5.50–5.44 (1H, m), 4.39 (1H, d, *J* = 17.5 Hz), 4.05 (3H, s), 3.99–3.90 (3H, m), 3.62–3.54 (1H, m), 3.39 (3H, s), 2.88–2.81 (1H, m), 2.24–2.15 (1H, m), 1.77 (1H, td, *J* = 13.7 Hz, *J* = 3.9 Hz); ^{13}C NMR (125.7 MHz, $CDCl_3$) δ: 162.2, 148.5, 148.3, 140.9, 134.3, 133.6, 133.1, 130.4, 129.3, 127.5, 122.3, 117.0, 101.0, 98.6, 89.3, 72.1, 63.2, 59.9, 59.2, 58.7, 56.6, 47.6, 28.8; ESI-HRMS *m*/*z* calcd for $C_{25}H_{24}N_3O_{10}^+$ $[M + H]^+$ 526.1456, found 526.1469.

2.3.6. 11-O-(2-Chlorobenzoyl)ambelline (23)

Yield 68 mg (96%); white powder; $[\alpha]_D^{24}$= +46.8 (*c* = 0.163; $CHCl_3$); ^{1}H NMR (500 MHz, $CDCl_3$) δ: 7.39–7.30 (2H, m), 7.22–7.12 (2H, m), 6.68 (1H, d, *J* = 10.0 Hz), 6.51 (1H, s), 6.09 (1H, dd, *J* = 10.0 Hz, *J* = 5.2 Hz), 5.80 (1H, d, *J* = 1.5 Hz), 5.76 (1H, d, *J* = 1.5 Hz), 5.32 (1H, dd, *J* = 8.1 Hz, *J* = 3.7 Hz), 4.37 (1H, d, *J* = 17.5 Hz), 3.98 (3H, s), 3.96–3.84 (3H, m), 3.50 (1H, dd, *J* = 13.7 Hz, *J* = 3.9 Hz), 3.36 (3H, s), 2.92–2.86 (1H, m), 2.19–2.11 (1H, m), 1.78 (1H, td, *J* = 13.7 Hz, *J* = 3.9 Hz); ^{13}C NMR (125.7 MHz, $CDCl_3$) δ: 165.1, 147.8, 140.6, 134.0, 133.9, 133.5, 132.5, 131.7, 131.4, 130.9, 129.3, 126.4, 126.1, 117.5, 100.5, 99.6, 88.6, 72.2, 63.5, 59.7, 59.1, 58.6, 56.5, 47.7, 28.8; ESI-HRMS: *m*/*z* calcd for $C_{25}H_{25}ClNO_6^+$ $[M + H]^+$ 470.1365, found 470.1373.

2.3.7. 11-O-(4-Chlorobenzoyl)ambelline (24)

Yield 65 mg (91%); white powder; $[\alpha]_D^{24}$= +13.0 (*c* = 0.185; $CHCl_3$); ^{1}H NMR (500 MHz, $CDCl_3$) δ: 7.61–7.54 (2H, m), 7.35–7.28 (2H, m), 6.60 (1H, d, *J* = 10.0 Hz), 6.52 (1H, s), 6.12–6.06 (1H, m), 5.86–5.78 (2H, m), 5.35 (1H, dd, *J* = 8.1 Hz, *J* = 3.8 Hz), 4.37 (1H, d, *J* = 17.5 Hz), 4.00 (3H, s), 3.93 (1H, overlap, d, *J* = 17.5 Hz), 3.92–3.84 (2H, overlap, m), 3.55–3.48 (m, 1H), 3.38 (3H, s), 2.83 (1H, ddd, *J* = 14.0 Hz, *J* = 4.0 Hz, *J* = 1.8 Hz), 2.22–2.14 (1H, m), 1.79 (1H, td, *J* = 14.0 Hz, *J* = 4.0 Hz); ^{13}C NMR (125.7 MHz, $CDCl_3$) δ: 165.4, 147.8, 140.7, 139.4, 133.9, 133.7, 131.3, 130.8, 128.5, 128.3, 126.7, 117.4, 100.5, 99.4, 88.1, 72.2, 63.3, 59.8, 59.2, 58.8, 56.6, 47.5, 28.8; ESI-HRMS: *m*/*z* calcd for $C_{25}H_{25}ClNO_6^+$ $[M + H]^+$ 470.1365, found 470.1371.

2.3.8. 11-O-(3-Bromobenzoyl)ambelline (25)

Yield 59 mg (72%); white powder; $[\alpha]_D^{24}$= +53.3 (*c* = 0.195; $CHCl_3$); ^{1}H NMR (500 MHz, $CDCl_3$) δ: 7.70–7.60 (2H, m), 7.56 (1H, t, *J* = 1.8 Hz), 7.28–7.21 (1H, m), 6.59 (1H, d, *J* = 10.0 Hz), 6.52 (1H, s), 6.10 (1H, dd, *J* = 10.0, *J* = 5.2 Hz), 5.89 (1H, d, *J* = 1.6 Hz), 5.84 (1H, d, *J* = 1.6 Hz), 5.37 (1H, dd, *J* = 8.1 Hz, *J* = 3.7 Hz), 4.38 (1H, d, *J* = 17.5 Hz), 4.03 (3H, s), 3.98–3.85 (3H, m), 3.55 (1H, dd, *J* = 13.5 Hz, *J* = 3.7 Hz), 3.38 (3H, s), 2.84 (1H, dd, *J* = 13.4, *J* = 3.7 Hz), 2.18 (1H, dd, *J* = 13.4, *J* = 3.7 Hz), 1.78 (1H, td, *J* = 13.5, *J* = 3.7 Hz); ^{13}C NMR (125.7 MHz, $CDCl_3$) δ: 164.9, 148.0, 140.8, 135.9, 134.1, 133.5, 132.5, 131.9, 131.1, 129.8, 128.0, 126.9, 122.2, 117.2, 100.7, 99.3, 87.9, 72.2, 63.2, 59.8, 59.3, 58.6, 56.6, 47.7, 28.7; ESI-HRMS: *m*/*z* calcd for $C_{25}H_{25}BrNO_6^+$ $[M + H]^+$ 514.0860, found 514.0867.

2.3.9. 11-O-(4-Methyl-3-nitrobenzoyl)ambelline (30)

Yield 76 mg (100%); pale yellow oil; $[\alpha]_D^{24}$= +78.7 (*c* = 0.122; $CHCl_3$); ^{1}H NMR (500 MHz, $CDCl_3$) δ: 7.97–7.95 (1H, m), 7.88 (1H, dd, *J* = 7.8 Hz, *J* = 1.5 Hz), 7.36 (1H, d, *J* = 7.8 Hz), 6.56 (1H, d, *J* = 10.0 Hz), 6.50 (1H, s), 6.09 (1H, dd, *J* = 10.0 Hz, *J* = 5.2 Hz), 5.91–5.89 (1H, m), 5.87–5.86 (1H, m), 5.40 (1H, dd, *J* = 8.0 Hz, *J* = 3.7 Hz), 4.38 (1H, d, *J* = 17.5 Hz), 4.02 (3H, s), 3.94 (1H, overlap, d, *J* = 17.5 Hz), 3.94–3.88 (2H, m, overlap), 3.55 (1H, dd, *J* = 13.8 Hz, *J* = 3.9 Hz), 3.37 (3H, s), 2.87–2.81 (1H, m), 2.62 (3H, s), 2.23–2.16 (1H, m), 1.78 (1H, td, *J* = 13.8 Hz, *J* = 3.9 Hz); ^{13}C NMR (125.7 MHz, $CDCl_3$) δ: 164.2, 149.0, 148.1, 140.7, 138.5, 134.1, 133.29, 133.25, 132.9, 130.9, 129.2, 126.9, 125.7, 117.0, 100.8, 99.0, 88.1, 72.1, 63.2, 59.8, 59.2, 58.6, 56.6, 47.6, 28.8, 20.6; ESI-HRMS: *m*/*z* calcd for $C_{26}H_{27}N_2O_8^+$ $[M + H]^+$ 495.1762, found 495.1771.

2.3.10. 11-O-(2-Chloro-4-nitrobenzoyl)ambelline (31)

Yield 91 mg (100%); yellow powder; $[\alpha]_D^{24}$ = -8.3 (*c* = 0.145; $CHCl_3$); ^{1}H NMR (500 MHz, $CDCl_3$) δ: 8.21 (1H, d, *J* = 2.1 Hz), 7.99 (1H, dd, *J* = 8.3 Hz, *J* = 2.1 Hz), 7.29 (1H, d, *J* = 8.3 Hz), 6.65 (1H, d, *J* = 9.9 Hz), 6.47 (1H, s), 6.10 (1H, dd, *J* = 9.9 Hz, *J* = 5.4 Hz), 5.82–5.79 (2H, m), 5.34 (1H, dd, *J* = 7.8 Hz, *J* = 3.5 Hz), 4.36 (1H, d, *J* = 17.6 Hz), 3.98 (3H, s), 3.94–3.85 (3H, m), 3.51 (1H, dd, *J* = 13.6 Hz, *J* = 3.5 Hz), 3.36 (3H, s), 2.94–2.87 (1H, m), 2.20–2.12 (1H, m), 1.75 (1H, td, *J* = 13.6 Hz, *J* = 3.5 Hz); ^{13}C NMR (125.7 MHz, $CDCl_3$) δ: 163.6, 149.3, 147.9, 140.7, 135.0, 134.9, 134.0, 133.3, 132.1, 131.3, 126.8, 125.9, 121.0, 117.6, 100.6, 99.2,

89.5, 72.1, 63.6, 59.6, 59.1, 58.5, 56.5, 47.9, 28.8; ESI-HRMS: *m*/*z* calcd for $C_{22}H_{29}NO_6^+$ $[M + H]^+$ 515.1216, found 515.1223.

2.3.11. 11-O-(4-Chloro-3-nitrobenzoyl)ambelline (32)

Yield 52 mg (59%); yellow powder; $[\alpha]_D^{24}$= +27.2 (*c* = 0.235; $CHCl_3$); ^{1}H NMR (500 MHz, $CDCl_3$) δ: 7.88 (1H, dd, *J* = 8.3 Hz, *J* = 2.0 Hz), 7.84 (1H, d, *J* = 2.0 Hz), 7.57 (1H, d, *J* = 8.3 Hz), 6.54 (1H, d, *J* = 10.1 Hz), 6.47 (1H, s), 6.14–6.06 (1H, m), 5.90–5.86 (2H, m), 5.32 (1H, dd, *J* = 8.1 Hz, *J* = 4.0 Hz), 4.37 (1H, d, *J* = 17.6 Hz), 4.02 (3H, s), 3.97–3.85 (3H, m), 3.56 (1H, dd, *J* = 13.7 Hz, *J* = 4.0 Hz), 3.37 (3H, s), 2.87–2.81 (1H, m), 2.23–2.16 (1H, m), 1.76 (1H, td, *J* = 13.7 Hz, *J* = 4.0 Hz); ^{13}C NMR (125.7 MHz, $CDCl_3$) δ: 163.3, 148.1, 147.6, 140.8, 134.1, 133.4, 133.2, 132.0, 131.7, 130.7, 129.8, 127.1, 126.5, 116.9, 100.9, 98.8, 88.4, 72.1, 63.2, 59.7, 59.2, 58.6, 56.6, 47.6, 28.7; ESI-HRMS *m*/*z* calcd for $C_{25}H_{24}ClN_2O_8^+$ $[M + H]^+$ 515.1216, found 515.1224.

2.3.12. 11-O-(3-Bromo-5-nitrobenzoyl)ambelline (33)

Yield 58 mg (69%); yellow powder; $[\alpha]_D^{24}$= +143.5 (*c* = 0.170; $CHCl_3$); ^{1}H NMR (500 MHz, $CDCl_3$) δ: 8.49 (1H, s), 8.24 (1H, s), 8.04 (1H, s), 6.55 (1H, d, *J* = 10.0 Hz), 6.50 (1H, s), 6.13 (1H, dd, *J* = 10.0 Hz, *J* = 5.2 Hz), 5.94–5.87 (2H, m), 5.50–5.44 (1H, m), 4.39 (1H, d, *J* = 17.5 Hz), 4.05 (3H, s), 3.99–3.90 (3H, m), 3.62–3.54 (1H, m), 3.39 (3H, s), 2.88–2.81 (1H, m), 2.24–2.15 (1H, m), 1.77 (1H, td, *J* = 13.6 Hz, *J* = 3.6 Hz); ^{13}C NMR (125.7 MHz, $CDCl_3$) δ: 162.2, 148.5, 148.3, 140.9, 134.3, 133.6, 133.1, 130.4, 129.3, 127.5, 122.3, 117.0, 101.0, 98.6, 89.3, 72.1, 63.2, 59.9, 59.2, 58.7, 56.6, 47.6, 28.8; ESI-HRMS *m*/*z* calcd for $C_{25}H_{24}BrN_2O_8^+$ $[M + H]^+$ 559.0711, found 559.0711.

2.4. In vitro experiments

2.4.1. Cell culture and culture conditions

Selected human tumour and non-tumour cell lines Jurkat (acute T cell leukemia), MOLT-4 (acute lymphoblastic leukemia), A549 (lung carcinoma), HT-29 (colorectal adenocarcinoma), PANC-1 (pancreas epithelioid carcinoma), A2780 (ovarian carcinoma), HeLa (cervix adenocarcinoma), MCF-7 (breast adenocarcinoma), SAOS-2 (osteosarcoma) and MRC-5 (non-tumour lung fibroblasts) were purchased from European Collection of Authenticated Cell Cultures (ECACC, Salisbury, UK) and cultured according to the provider's culture method guidelines. All cell lines were maintained at 37 °C in a humidified 5% carbon dioxide and 95% air incubator. The cells in low passage number (non-tumour primary cell line MRC-5 was used for a maximum of 10 passages and cancer cell lines were used for a maximum of 20 passages) and in an exponential growth phase were used for this study.

2.4.2. WST-1 cell proliferation assay, growth percent calculation and IC_{50} value determination

Each cell line was seeded at a previously established optimal density (1.10^3 to 50.10^3 cells per well) in a 96-well plate (TPP, Trasadingen, Switzerland) and cells were allowed to settle overnight. In initial screening tests, cells were treated for 48 h with either ambelline or the newly synthesized derivative compounds at a final concentration of 10 μM. The 50% inhibitory concentration (IC_{50}) values for the most active compounds were determined using the concentration range from 1 to 50 μM with the treatments for 48 h before assay to determine cell proliferation. Doxorubicin (Sigma-Aldrich, St. Louis, USA), at a concentration of 1 μM, was used as a positive control. At the end of the culture period, the WST-1 proliferation assay (Roche, Basel, Switzerland) was performed according to the manufacturer's protocol. The absorbance was determined using a Tecan Spark microplate reader (Tecan, Männedorf, Switzerland). Each value is the mean of three independent experiments and represents the percentage of the proliferation of control, non-treated cells (100%). The growth percent (GP) value was calculated for each derivative tested. GP represents the mean of the proliferation decrease percentage of all the 10 cell lines treated with the exact ambelline derivative. IC_{50} values were calculated based on data obtained from proliferation determined by a WST-1 assay and were processed using GraphPad Prism7 biostatistics (GraphPad Software, San Diego, CA, USA) software. Drug concentrations were plotted against the cell proliferation/viability percentage, and the IC_{50} values were determined using nonlinear regression.

2.4.3. Screening for antiproliferative activity using xCELLigence system

The xCELLigence system (Roche, Basel, Switzerland and ACEA Biosciences, San Diego, CA, USA) was used to monitor cell adhesion, proliferation and cytotoxicity. The xCELLigence system was connected and tested by Resistor Plate before the real-time cell analysis (RTCA) Single Plate station was placed inside the incubator at 37 °C and 5% CO_2. First, the optimal seeding concentration for experiments was optimized for each cell line. After seeding the respective number of cells in 190 μL medium per well of the E-plate 96, the impedance was recorded every 30 min. Approximately 24 h after seeding, when the cells were in the log growth phase, the cells were exposed in triplicates to 10 μL sterile deionized water containing ambelline derivatives to obtain final concentrations 1–50 μM. Controls received sterile deionized water + dimethyl sulfoxide (DMSO) with a final concentration of 0.1%. Cells treated with 5% DMSO were used as a positive control. Growth curves were normalized to the time point of treatment. Evaluations were performed using xCELLigence 1.2.1 software (Roche, Basel, Switzerland and ACEA Biosciences, San Diego, CA, USA).

2.4.4. Proliferation and viability measurement using Trypan blue exclusion test

A Trypan blue exclusion assay was used for measuring cell proliferation and viability. The cells were treated with varying concentrations (1, 2, 5, and 10 μM) of **10**, **16** and **32** and further cultured for 24 h and 48 h in the case of both MOLT-4 and Jurkat cells. Cells treated with 0.25 μM doxorubicin were used as a positive control. Cell membrane integrity was determined using the Trypan blue exclusion technique – mixing 10 μL of 0.4% Trypan blue and 10 μL of cell suspension. Cell counts were carried out using a Bürker chamber and a Nikon Eclipse E200 light microscope (Nikon, Tokyo, Japan).

2.4.5. Cell cycle and internucleosomal DNA fragmentation analysis

Cultured cells were collected, washed with ice-cold phosphate-buffered saline (PBS; Sigma-Aldrich, St. Louis, MO, USA), fixed with 70% ethanol and stored at 4 °C for subsequent cell cycle distribution analysis. Afterwards, fixed cells were centrifuged to remove ethanol and washed with ice-cold PBS twice. In order to detect low molecular-weight fragments of DNA, the cells were incubated for 5 min at room temperature in a buffer (192 mL 0.2 M Na_2HPO_4 + 8 mL of 0.1 M citric acid, pH 7.8) and then, after washing the cells with ice-cold PBS, labelled with propidium iodide in Vindelov's solution for 1 h at 37 °C. The DNA content was determined by using a CytoFLEX LX flow cytometer (Beckman Coulter, Miami, FL, USA) with an excitation wavelength of 488 nm. The data were analysed using Kaluza Analysis 2.1 software (Beckman Coulter, Miami, FL, USA).

2.4.6. Flow cytometry quantification of apoptosis by Annexin V/PI double staining

Apoptosis was determined by flow cytometry using an Alexa Fluor® 488 Annexin V/Dead Cell Apoptosis kit (Life Technologies, Grand Island, NY, USA), in accordance with the manufacturer's

instructions. This kit employs the property of Alexa Fluor®488 conjugated to Annexin V to bind to phosphatidylserine in the presence of Ca^{2+}, and the ability of propidium iodide (PI) to enter cells with damaged cell membranes and bind to DNA. Measurement was performed using a CytoFLEX LX Flow Cytometer (Beckman Coulter, Miami, FL, USA). List mode data were analysed using Kaluza Analysis 2.1 software (Beckman Coulter, Miami, FL, USA).

2.4.7. Activity of caspase-3 and caspase-7

The induction of apoptosis was determined by monitoring the activity of caspase-3/-7 by Caspase-Glo Assays (Promega, Madison, WI, USA) 24 h after treatment with 2 and 3 μM of derivatives **10**, **16** and **32**. Cells treated with 1 μM of doxorubicin were used as a positive control. The assay provides a proluminogenic substrate in an optimized buffer system. The addition of a Caspase-Glo Reagent results in cell lysis, followed by caspase cleavage of the substrate and the generation of a luminescent signal. A total of 1×10^4 cells was seeded per well using a 96-well-plate format (Sigma-Aldrich, St. Louis, MO, USA). After treatment, the Caspase-Glo Assay Reagent was added to each well (100 μL per well) and incubated for 30 min before luminescence was measured using a Tecan Spark microplate reader (Tecan Group, Männedorf, Switzerland).

2.5. Statistical analysis

The descriptive statistics of the results were calculated, and charts were made using either Microsoft Office 365 Excel (Microsoft, Redmond, WA, USA) or GraphPad Prism 7 biostatistics (GraphPad Software, La Jolla, CA, USA) software. In this study, all the values were expressed as arithmetic means with SD of triplicates, unless otherwise noted. For quantitative data, normality testing was performed to assess whether parametric or nonparametric tests should be used. For experiments with parametric variables, significant differences between the groups were analysed using the Student's T-test and a P value $\leq$ 0.05 was considered significant.

3. Results

3.1. Preparation of ambelline (1) derivatives (10, 14, 16, 17, 22–25, 30–33)

To extend our library of ambelline derivatives (Marikova et al., 2020), and describe the SAR in more depth, twelve further derivatives were synthesized. All newly synthesized derivatives were modified by binding aromatic ligands at the C-11 hydroxyl group of ambelline (**1**), using differently substituted benzoyl chlorides affording the corresponding esters (Fig. 2). Data from MS, HRMS, and NMR analyses confirmed the structures of the designed compounds (see Supplementary Material for spectra).

3.2. Cytotoxicity screening of previously and newly developed ambelline derivatives

The antiproliferative effect of the totally synthesized compounds and of the parent ambelline were quantified in a panel of cell lines derived from various human tumour types (leukemia-Jurkat, MOLT-4; lung adenocarcinoma-A549, colon-HT-29, pancreas-PANC-1, cervix-HeLa, breast-MCF-7; ovarian carcinoma-A2780, and osteogenic sarcoma-SAOS-2). The effect on non-tumour cells was tested using primary human fetal lung fibroblasts (MRC-5). Exposure of the cell lines to the compounds (**1–33**) lasted for 48 h, and the changes in cell proliferation compared to the untreated control were determined using WST-1 assay based on mitochondrial dehydrogenase activities. The antiproliferative effect of parent ambelline was identical to that previously described (Havelek et al., 2017). The antiproliferative effect of each tested compound across the various cell lines is expressed in a separate graph, and the horizontal line intersects the bar graphs at 50% inhibition of proliferation (Fig. 3).

As shown in Fig. 3 and Table 1, none of the aliphatic esters (**2–5**), nor ambelline (**1**) itself, demonstrated any cytotoxic activity (cell viability around 100%). The screened aromatic esters of ambelline were divided into five structurally related groups. The simple 11-*O*-benzoylambelline (**6**) was only mildly cytotoxic to Jurkat cells, but its methyl derivatives (**7–10**), forming the first group of aromatic esters of ambelline modified by methyl group/-groups attached to the phenyl, showed less histotype-specific potency. In particular, 11-*O*-(3-methylbenzoyl)ambelline (**8**) showed preferential antiproliferative activity against acute T-cell leukemia, ovarian and bone cancer cells. Speaking of disubstituted derivatives, the cytotoxic activity of 11-*O*-(3,5-dimethylbenzoyl) ambelline (**10**) was extended to almost the entire spectrum of tested tumour cell lines. Following the methylbenzoyl derivatives, a scaffold with methoxybenzoyl was evaluated (**11–18**). In general, disubstituted benzoyl derivatives showed the most pronounced activity with methoxy functional groups in different positions (**14–16**). Cytotoxic activity was even more enhanced by

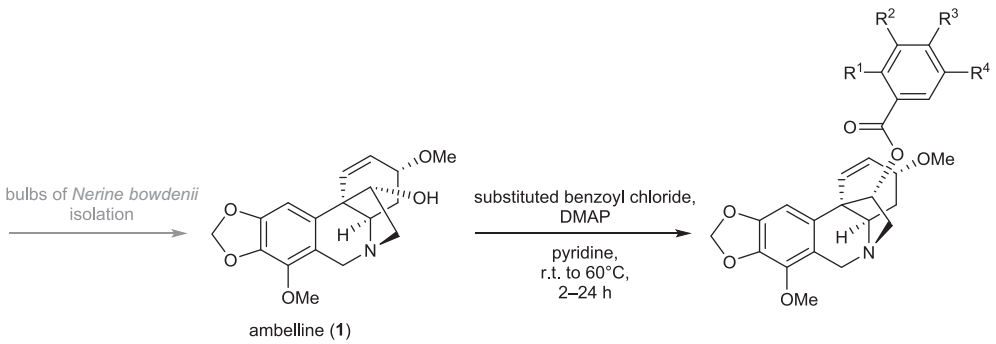

10: R^1=H, R^2=Me, R^3=H, R^4=Me
14: R^1=OMe, R^2=H, R^3=OMe, R^4=H
16: R^1=H, R^2=OMe, R^3=H, R^4=OMe
17: R^1=H, R^2=OMe, R^3=OMe, R^4=OMe
22: R^1=H, R^2=NO_2, R^3=H, R^4=NO_2
23: R^1=Cl, R^2=H, R^3=H, R^4=H
24: R^1=H, R^2=H, R^3=Cl, R^4=H
25: R^1=H, R^2=Br, R^3=H, R^4=H
30: R^1=H, R^2=NO_2, R^3=Me, R^4=H
31: R^1=Cl, R^2=H, R^3=NO_2, R^4=H
32: R^1=H, R^2=NO_2, R^3=Cl, R^4=H
33: R^1=H, R^2=Br, R^3=H, R^4=NO_2

Fig. 2. Design and synthesis of new ambelline derivatives.

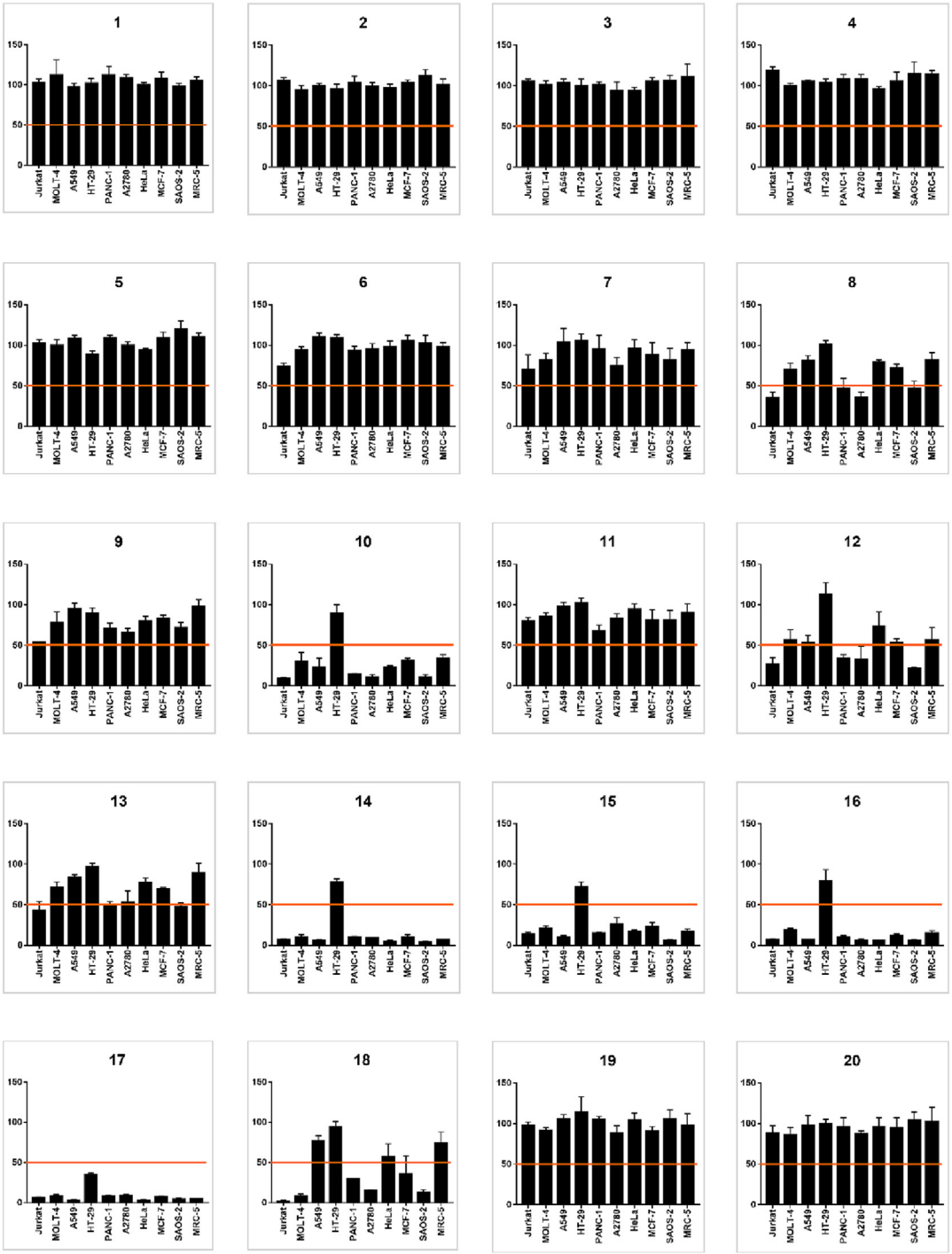

Fig. 3. Inhibition of proliferation using all tested compounds treatment (**1–33**, positive control 1 μM doxorubicin). Each compound was tested on ten cell lines and this effect is presented in a separate graph. The antiproliferative activity after the treatment at 10 μM for 48 h was measured using WST-1 assay and expressed as a percentage of control cells (0.1% DMSO treated, proliferation 100%). Each value represents the mean ± standard deviation of three independent experiments. The horizontal line highlights the 50% value.

trimethoxybenzoyl substitution (**17**). These derivatives were also active on the doxorubicin-resistant cell line PANC-1 but had only medium growth inhibitory activity on HT-29. In contrast, the cytotoxic activity was decreased by changing the methoxy groups to ethoxy groups (**18**). Nitro derivatives (**19–22**) did not show any significant cytotoxicity. Surprisingly, this was the case even with 11-*O*-(3,5-dinitrobenzoyl)ambelline (**22**), which is analogous to a haemanthamine derivative which had an amplified effect on the whole tumour cell line spectra (Uher et al., 2022). A similar trend of higher cytotoxic potential did not occur in the case of more substituted aromatic rings, such as previously described groups. Halogen derivatives having 2-chloro (**23**), 4-chloro (**24**), or 1-bromo (**25**) benzoyl substitution showed no cytotoxic potential at all. Naphtoyl and furoyl derivatives were synthesized as the next group of derivatives (**26–29**). Comparing this group of derivatives, compound **26** was the least effective against cancer cell lines. Both furoyl derivatives (**28**, **29**) and 11-*O*-(2-naphtoyl)ambelline (**27**) were active by the same magnitude against Jurkat leukemic cells.

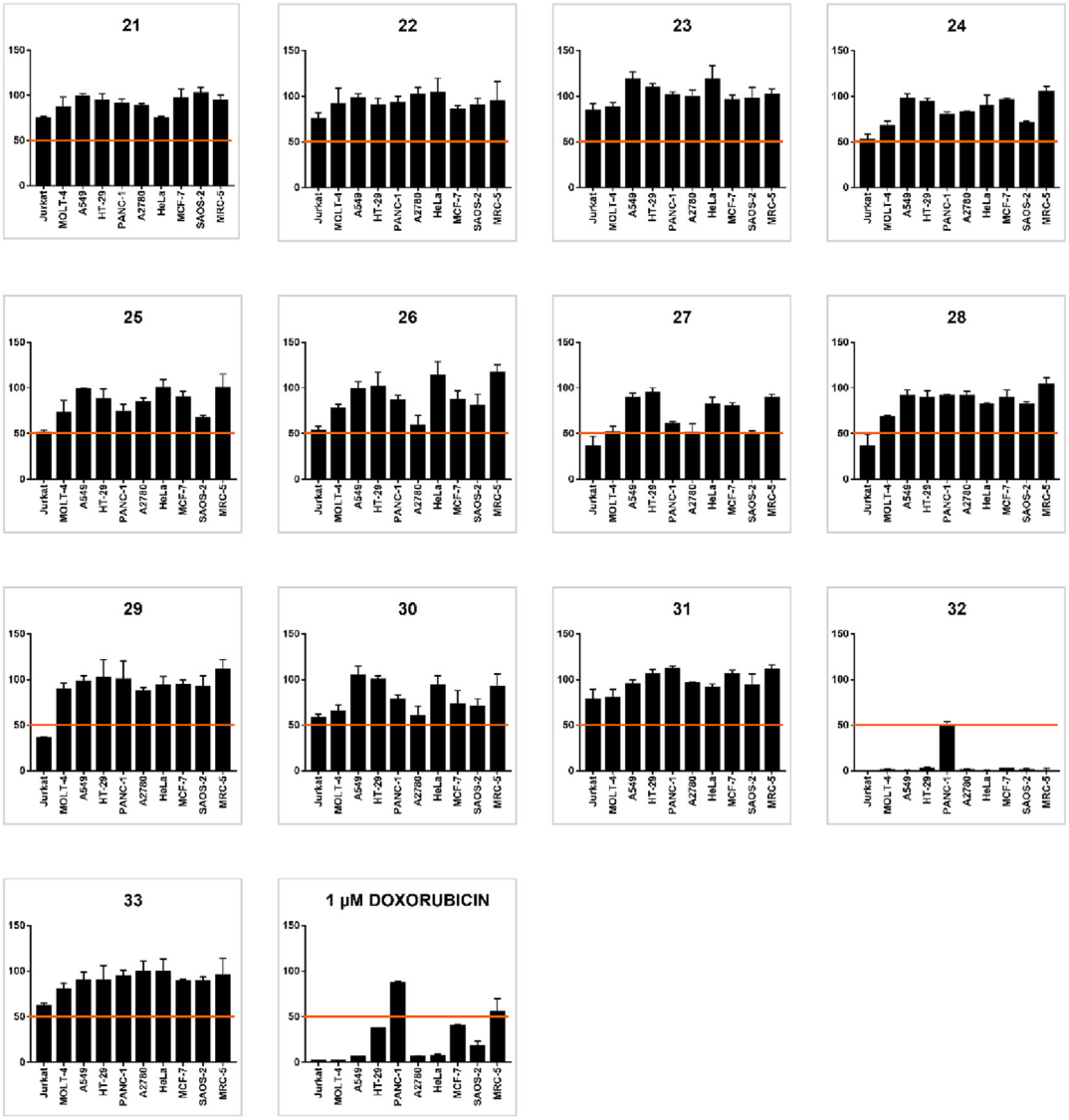

Fig. 3 (*continued*)

The last group contains derivatives with different disubstitutions on the aromatic ring (**30–33**). Inspiration for the preparation of this group is related to our previous publication describing derivatives of haemanthamine (Uher et al., 2022). All these compounds contain a combination of a nitro group with either halogen or methyl functional groups. Among all derivatives in this study, 11-*O*-(4-chloro-3-nitrobenzoyl)ambelline (**32**) was the most active compound, which also showed growth inhibition of the doxorubicin-resistant HT-29 cell line**.** Interestingly, 3-nitro (**20**) and 4-chloro (**24**) derivatives were inactive. Changing the position of chlorine to *para* on the aromatic ring to the methyl group significantly reduced the cytotoxicity.

As summarized in Tables 1 and 2, the mean growth percent (GP) value of the derivative **32** is 6%, ranging from 0 to 49%, with the most effective inhibition on HeLa, MRC-5, and Jurkat cell lines. All cell lines were susceptible (GP value 0–2%), except for PANC-1 (GP value 49%), which is resistant to the standard cytostatic doxorubicin. The disubstituted methoxy derivative **16** exhibited potent inhibitory activities toward the cancer cell lines, with GP values spanning from 6% to 19%, excluding a GP of 79% obtained on HT-29. By contrast, disubstituted methylbenzoyl derivative **10** displayed a slight decline in activity. Notably, derivative **10** showed GP values from 0 to 25% and was highly cytotoxic towards Jurkat, A549, PANC-1, A2780, HeLa, and SAOS-2 cells lines, while only marginally affecting (GP range above 26%) MOLT-4, HT-29, MCF-7, and MRC-5 cells. Trimethoxy derivative **17**, with a mean GP value of 9%, is potent to the doxorubicin-resistant PANC-1 cell line. Furthermore, the derivative **17** reduced the proliferation of the resistant colon carcinoma HT-29 to a similar level as that of the standard cytostatic doxorubicin.

Values of IC_{50} determined for the selected ambelline derivatives (**8**, **10, 14**–**18, 27–29, 32**) are summarized in Table 3. The cytotoxicity screening showed that ambelline derivatives from the methylbenzoyl group (**10**), the methoxybenzoyl group (**16** and **17**), and the group of compounds with different disubstitution on the aromatic ring (**32**) appear to be most effective. Their concurring feature seems to be either a disubstitution in the *meta* positions (**10**, **16**) or a disubstitution in the *meta* and *para* positions (**17**, **32**) of the benzoyl ring. However, since these substituents have a different chemical nature (meaning electronic effect and density, or molecular weight in general), the influence of the substituent itself is not entirely clear. To gain a deeper understanding of the antiproliferative effects of the three most advantageous derivatives (**10**, **16**, **32**), cytotoxicity screening was further extended with

Table 1
Growth percentage (GP) values of each compound and doxorubicin for all cell lines were determined after the application of 10 μM concentration of treatment using 48 h time of incubation and detected by the WST-1 method, related to the negative control cells (0.1% DMSO treated, proliferation 100 %). Each value is a mean of three independent experiments. Values from the intervals 0–25%, 26–50%, and 51–75% are counterpointed with different colours. Doxorubicin at 1 μM was used as a reference drug.

	Jurkat	MOLT-4	A549	HT-29	PANC-1	A2780	HeLa	MCF-7	SAOS-2	MRC-5
Ambelline (1)	103	112	97	102	112	109	100	108	98	105
2	106	95	100	96	104	99	97	104	112	101
3	105	101	104	100	101	94	94	105	106	111
4	119	100	105	104	108	108	96	105	115	114
5	102	100	108	89	109	100	94	109	120	110
6	74	94	110	109	93	95	98	106	102	98
7	70	82	104	106	95	75	96	88	82	94
8	35	70	81	101	47	36	79	72	47	82
9	54	78	95	89	71	65	80	83	72	98
10	9	30	23	89	14	11	23	31	11	34
11	80	86	98	102	67	83	94	81	81	90
12	27	57	53	113	34	33	73	53	21	57
13	46	71	83	97	50	53	77	69	47	89
14	7	10	6	78	10	9	5	10	4	7
15	14	21	10	72	15	26	17	23	6	17
16	7	19	7	79	10	6	6	12	6	15
17	6	8	3	35	8	9	3	7	4	5
18	2	8	77	94	29	15	57	36	13	74
19	98	92	106	114	105	88	104	91	106	98
20	88	86	98	100	96	87	96	94	104	102
21	75	87	99	94	91	88	75	97	102	94
22	75	91	98	90	93	102	104	86	90	95
23	84	88	118	110	101	99	118	96	97	102
24	52	67	97	94	80	82	89	96	71	105
25	51	73	98	88	74	84	100	90	67	100
26	53	77	98	101	86	59	113	87	81	117
27	36	52	89	95	60	51	82	80	50	89
28	36	68	91	89	91	91	82	89	82	104
29	36	89	98	102	100	87	93	94	92	111
30	58	65	105	100	78	60	93	73	70	92
31	78	80	95	106	112	96	91	106	93	111
32	0	1	0	2	49	1	0	2	1	0
33	62	80	90	90	94	100	100	89	89	95
DOX	2	2	6	37	87	6	7	40	18	56

0-25% **26-50%** **51-75%**

complementary techniques focused on dynamic cell proliferation, viability, cell cycle distribution pattern, and apoptosis in the selected cancer cell models (Fig. 4).

3.3. Determination of the antiproliferative activity on selected cancer cell lines monitored in real-time using the xCELLigence system

To verify further the antiproliferative activity of the ambelline derivatives associated with the most effective inhibition, we performed dynamic real-time proliferation monitoring by the xCELLigence system. The xCELLigence system dynamically observes cell proliferation, morphology, adhesion, and viability based on impedance measurement. Impedance changes are expressed as normalized cell index (CI) values. As shown in Fig. 5**A and B**, the application of derivatives **10** and **16** decreased the proliferation of human lung carcinoma (A549), ovarian carcinoma (A2780), breast adenocarcinoma (MCF-7), and non-cancer human fetal lung fibroblast (MRC-5) cells in dose-dependent manners during the investigated 72 h interval. The decrease was more manifested in MCF-7 and A2780 cells.

Consistent with the previous data, the results of xCELLigence monitoring of cell growth in real-time, as shown in Fig. 5**C**, indicated that derivative **32** (20 and 50 μM) had a negative impact on A549, A2780, and MCF-7 cell proliferation. Exposure to derivative **32** at 20 μM and 50 μM resulted in an almost complete reduction in cell proliferation. The A549, A2780, and MCF-7 cells treated with lower doses (1, 5, and 10 μM) of derivative **32** were either unaffected or showed only slightly decreased proliferation. In

Table 2
The table summarizes the mean growth percentage (GP), including its lowest and highest values, and depicts the three most responsive cell lines. The GP value of each compound represents the average of the proliferation after the application of a 10 μM dose within a 48 h treatment time interval on ten cell lines. Data were calculated from three independent experiments and are expressed as a percent of the proliferation of 0.1% DMSO mock-treated control cells (100%).

Ambelline derivative		Mean GP	Range of GP	Three most sensitive cell lines
1	Ambelline	104	97–112	A549, SAOS-2, HeLa
2	11-*O*-acetylambelline	101	95–112	MOLT-4, HT-29, HeLa
3	11-*O*-propionylambelline	102	94–111	A2780, HeLa, HT-29
4	11-*O*-isobutanoylambelline	108	96–119	HeLa, MOLT-4, HT-29
5	11-*O*-pentanoylambelline	104	89–120	HT-29, HeLa, A2780
6	11-*O*-benzoylambelline	98	74–110	Jurkat, PANC-1, MOLT-4
7	11-*O*-(2-methylbenzoyl)ambelline	89	70–106	Jurkat, A2780, MOLT-4
8	11-*O*-(3-methylbenzoyl)ambelline	65	35–101	Jurkat, A2780, SAOS-2
9	11-*O*-(4-methylbenzoyl)ambelline	79	54–98	Jurkat, A2780, PANC-1
10	11-*O*-(3,5-dimethylbenzoyl)ambelline	28	9–89	Jurkat, SAOS-2, A2780
11	11-*O*-(2-methoxybenzoyl)ambelline	86	67–102	PANC-1, Jurkat, MCF-7
12	11-*O*-(3-methoxybenzoyl)ambelline	52	21–113	SAOS-2, Jurkat, A2780
13	11-*O*-(4-methoxybenzoyl)ambelline	68	43–97	Jurkat, SAOS-2, PANC-1
14	11-*O*-(2,4-dimethoxybenzoyl)ambelline	15	4–78	SAOS-2, HeLa, A549
15	11-*O*-(3,4-dimethoxybenzoyl)ambelline	22	6–62	SAOS-2, A549, Jurkat
16	11-*O*-(3,5-dimethoxybenzoyl)ambelline	17	6–79	HeLa, SAOS-2, A2780
17	11-*O*-(3,4,5-trimethoxybenzoyl)ambelline	9	3–35	A549, HeLa, SAOS-2
18	11-*O*-(3,5-diethoxybenzoyl)ambelline	40	2–94	Jurkat, MOLT-4, SAOS-2
19	11-*O*-(2-nitrobenzoyl)ambelline	100	88–114	A2780, MCF-7, MOLT-4
20	11-*O*-(3-nitrobenzoyl)ambelline	95	86–104	MOLT-4, A2780, Jurkat
21	11-*O*-(4-nitrobenzoyl)ambelline	90	75–102	Jurkat, HeLa, MOLT-4
22	11-*O*-(3,5-dinitrobenzoyl)ambelline	92	75–104	Jurkat, MCF-7, HT-29
23	11-*O*-(2-chlorobenzoyl)ambelline	101	84–118	Jurkat, MOLT-4, MCF-7
24	11-*O*-(4-chlorobenzoyl)ambelline	83	52–105	Jurkat, MOLT-4, SAOS-2
25	11-*O*-(3-bromobenzoyl)ambelline	83	51–100	Jurkat, SAOS-2, MOLT-4
26	11-*O*-(1-napthoyl)ambelline	87	53–117	Jurkat, A2780, MOLT-4
27	11-*O*-(2-napthoyl)ambelline	68	36–95	Jurkat, SAOS-2, MOLT-4
28	11-*O*-(2-furoyl)ambelline	82	36–104	Jurkat, MOLT-4
29	11-*O*-(3-furoyl)ambelline	90	36–111	Jurkat, MOLT-4, A2780
30	11-O-(4-methyl-3-nitrobenzoyl)ambelline	79	58–105	Jurkat, A2780, MOLT-4
31	11-*O*-(2-chloro-4-nitrobenzoyl)ambelline	97	78–112	Jurkat, MOLT-4, HeLa
32	11-*O*-(4-chloro-3-nitrobenzoyl)ambelline	6	0–49	HeLa, MRC-5, Jurkat
33	11-*O*-(3-bromo-5-nitrobenzoyl)ambelline	89	62–100	Jurkat, MOLT-4, MCF-7

Table 3
IC_{50} (μM) for the most active ambelline derivatives (results are the mean values ± standard deviations of at least - three independent replications).

Cell line	8	10	12	13	14	15	16	17	18	27	28	29	32
Jurkat	>10	2.2 ± 0.3	>10	>10	2.3 ± 0.4	3.0 ± 0.3	1.2 ± 0.2	1.1 ± 0.9	3.3 ± 0.3	9.2 ± 0.1	>10	>10	2.7 ± 0.1
MOLT-4	>10	>10	>10	>10	4.2 ± 0.2	7.4 ± 0.1	7.0 ± 0.6	2.9 ± 0.3	7.6 ± 0.1	>10	>10	>10	1.9n ± 01
A549	>10	5.0 ± 0.4	>10	>10	1.9 ± 0.5	2.6 ± 0.4	2.3 ± 0.2	1.7 ± 0.6	>10	>10	>10	>10	0.8 ± 0.1
HT-29	>10	>10	>10	>10	>10	>10	>10	>10	>10	>10	>10	>10	1.4 ± 0.2
PANC-1	>10	3.6 ± 0.6	8.7 ± 1.1	>10	1.3 ± 0.8	2.3 ± 0.4	1.5 ± 0.2	1.2 ± 0.8	8.3 ± 0.1	>10	>10	>10	9.9 ± 0.2
A2780	>10	4.8 ± 0.3	>10	>10	3.1 ± 0.3	6.0 ± 0.2	1.0 ± 0.3	2.3 ± 0.4	7.8 ± 0.1	>10	>10	>10	3.2 ± 0.1
HeLa	>10	7.7 ± 0.7	>10	>10	2.5 ± 0.4	4.8 ± 0.2	2.7 ± 0.2	3.0 ± 0.3	5.0 ± 0.2	>10	>10	>10	0.7 ± 0.2
MCF-7	>10	8.5 ± 0.7	>10	>10	7.6 ± 0.1	4.9 ± 0.2	2.8 ± 0.5	2.5 ± 0.4	6.3 ± 0.1	>10	>10	>10	0.6 ± 0.1
SAOS-2	>10	2.3 ± 0.3	6.9 ± 1.0	>10	1.1 ± 0.9	2.1 ± 0.5	1.1 ± 0.1	1.0 ± 1.0	2.8 ± 0.4	>10	>10	>10	2.3 ± 0.1
MRC-5	>10	>10	>10	>10	4.1 ± 0.2	6.1 ± 0.2	3.6 ± 0.3	2.3 ± 0.4	>10	>10	>10	>10	0.7 ± 0.1

contrast, the proliferation of MRC-5 cells was not significantly affected by the treatment with derivative **32** within the 1–20 μM dose range.

Only MRC-5 cells treated with derivative **32** at the highest evaluated dose of 50 μM showed a complete reduction of cell proliferation with a constantly decreased cell index.

3.4. Determination of the inhibitory effect of 10, 16, and 32 on MOLT-4 Jurkat cells by the tryptan blue exclusion assay

To find out if the inhibitory effect of **10**, **16**, and **32** on MOLT-4 Jurkat cells is associated with antiproliferation and/or the loss of cell viability, the Trypan blue exclusion assay was performed. As shown in Fig. 6**A**, incubating cells with 5 and 10 μM of **32** for 48 h led to complete growth inhibition in MOLT-4 cells, but did not show such a pronounced effect in Jurkat cells. The results, summarized in Fig. 6**B**, also indicated that cell viability was considerably reduced by compound **32** treatment at 5 and 10 μM. Above all, MOLT-4 cells showed the highest sensitivity to exposure to **32**, resulting in an almost complete loss of cell viability. Concerning derivatives **10** and **16**, they failed to show distinct antiproliferative and cell viability-decreasing effects at a concentration of up to 10 μM.

3.5. Treatment with 10, 16, and 32 had no effect on cell cycle phase distribution in MOLT-4 cells

Aiming to determine whether **10**, **16**, and **32** treatments for 24 h could modulate the cell cycle, flow cytometry was used to appraise the cycle progression in MOLT-4 cells. As shown in Fig. 7, no significant effect on cell cycle progression was observed relative to the 0.1% DMSO sham-treated negative control sample. However,

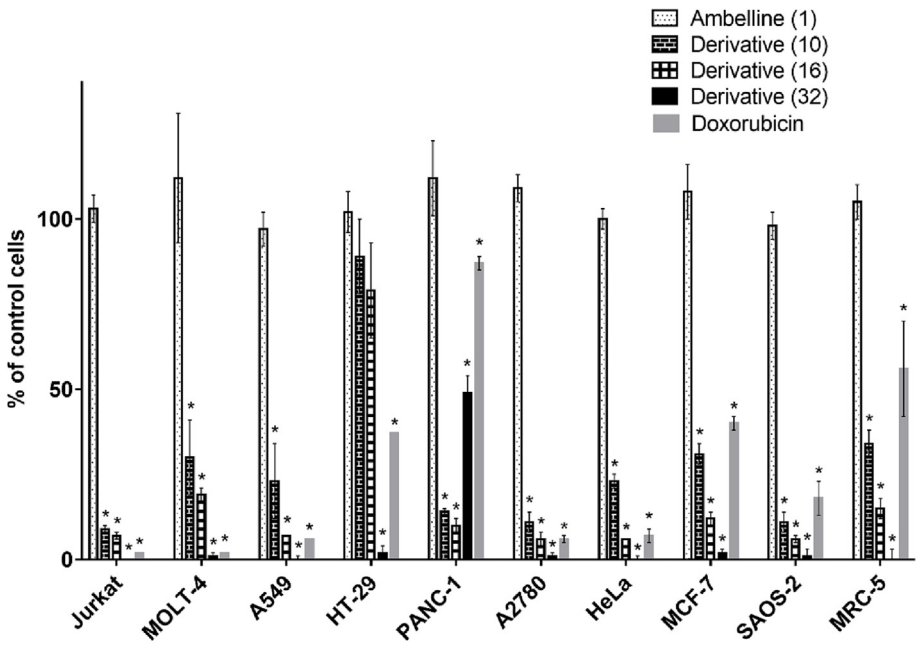

Fig. 4. Cytotoxic activity of ambelline (**1**) and derivatives **10**, **16**, and **32** upon exposure to a single dose of 10 μM. Cell proliferation was assessed using a WST-1 tetrazolium-based assay 48 h after treatment. The results are expressed as means ± SD of a minimum of three independent experiments (n = 3). Cells treated with the conventional cytotoxic agent doxorubicin dosed at 1 μM were used as a positive control. * $P \leq 0.05$ versus 0.1% DMSO sham-treated control.

treatment with 5 and 10 μM of **32** for 24 h resulted in a marked increase in cell death and a striking reduction in cell number, as observed by flow cytometric analysis. Unfortunately, investigating cell cycle transitions was not possible using this method.

3.6. Compound 32 causes apoptosis in a caspase-dependent manner

The ability of **10**, **16**, and **32** dosed at 2 and 3 μM to promote apoptosis was determined by flow cytometry after staining MOLT-4 cells with Annexin V-Alexa Fluor® 488 and propidium iodide (PI). Annexin V/PI double staining allowed us to separate the percentage (%) of Annexin V/PI-negative (viable) cells, Annexin V-positive and PI-negative (early apoptotic) cells, and Annexin V- and PI-positive (the late phase apoptotic) cells, while Annexin V-negative and PI-positive (necrotic) cells were excluded. The results summarized in Fig. 8 show that the positive control, cisplatin, applied at 5 μM and ambelline derivative **32**, applied at 3 μM, significantly ($p \leq 0.05$) induced apoptosis in MOLT-4 cells. Treatment with **32** at 3 μM induced a higher incidence of early apoptotic cells (12 %) and late apoptotic cells (39 %). Moreover, when MOLT-4 cells were exposed to cisplatin for 24 h, the cells in the early apoptotic state increased from 3 % (negative control) to 14 % (cisplatin), and the cells in the late apoptotic state increased from 4 % (negative control) to 29 % (cisplatin).

Considering derivative **32** as an active compound capable of inducing programmed cell death in MOLT-4 cells, measurement of the activity of effector caspase-3/-7, which is responsible for the successful course of apoptosis, was used to delineate whether apoptosis induced by **32** was executed via caspase proteins activation. As depicted in Fig. 9, the treatment with **32** at 3 μM for 24 h resulted in a significant increase in activity of caspase-3/-7 expressed in percent compared to a negative control (0,1 % DMSO-mock treated cells, 100 %). This finding corresponds to the results of quantification by Annexin V/PI staining, where the derivative **32** at 3 μM significantly induced a higher incidence of apoptosis in MOLT-4 cells. These pieces of evidence are consistent with previous experimental work on Amaryllidaceae alkaloids.

4. Discussion

Regarding biological activities, a more detailed understanding of representatives derived from the structure of β-crinane is at the beginning. According to current data, this scaffold shows a lower ability to inhibit the growth and viability of cancer cell lines than stereoisomers of α-crinane since haemanthamine as a model α-crinane has shown cytotoxic properties with a promising potential in antitumor therapy (Havelek et al., 2014; Cahlikova et al., 2021). But on the other hand, some studies suggested that β-crinane derivatives deserve more attention in studying the cytotoxic activity of isoquinoline alkaloids (Nair et al., 2014; 2016a, 2016b). Initially, attention was focused on distichamine, augustine, buphanisine, and ambelline because of their considerable cytostatic and cytotoxic effects (Ding et al., 2017; Havelek et al., 2017).

Thus, earlier studies demonstrated that β-crinane Amaryllidaceae alkaloids are valuable compounds for semisynthetic modifications because they themselves showed some antiproliferative properties against human cancer cells. The cytotoxic activity of β-crinane distichamine was studied on a mini-panel of human cell cultures 72 h after exposure. In this model, distichamine showed cytotoxic activity against the cell line CEM (IC_{50} = 4.5 ± 1.6 μM), K562 (IC_{50} = 4.1 ± 0.9 μM), MCF-7 (IC_{50} = 2.3 ± 0.8 μM), HeLa (IC_{50} = 2.2 ± 0.1 μM), G-361 (IC_{50} = 14.7 ± 0.1 μM) and non-tumour BJ fibroblasts (IC_{50} = 10.5 ± 1.9 μM). More detailed studies of the cytotoxicity mechanism of distichamine in the concentration range of 1–20 μM in a treatment period of 24 h on CEM acute lymphoblastic leukemia cells demonstrated an antiproliferative and cytotoxic effect with the accumulation of cells in the G2 phase of the cell cycle and the induction of apoptosis through the activation of caspase-3 and caspase-7 (Nair et al., 2016b). The currently barely studied β-crinane alkaloid augustine showed cytotoxic activity (within an exposure interval of 48 h) with a value of 50% inhibitory concentration ED_{50} against cells of epithelial carcinoma KB (0.6 μg/mL), glioblastoma U373 (0.6 μg/mL), breast carcinoma BCA-1 (2.8 μg/mL), colorectal carcinoma COL-1 (2.4 μg/mL), fibrosarcoma HT-1080 (1.2 μg/mL), lung carcinoma LUC-1

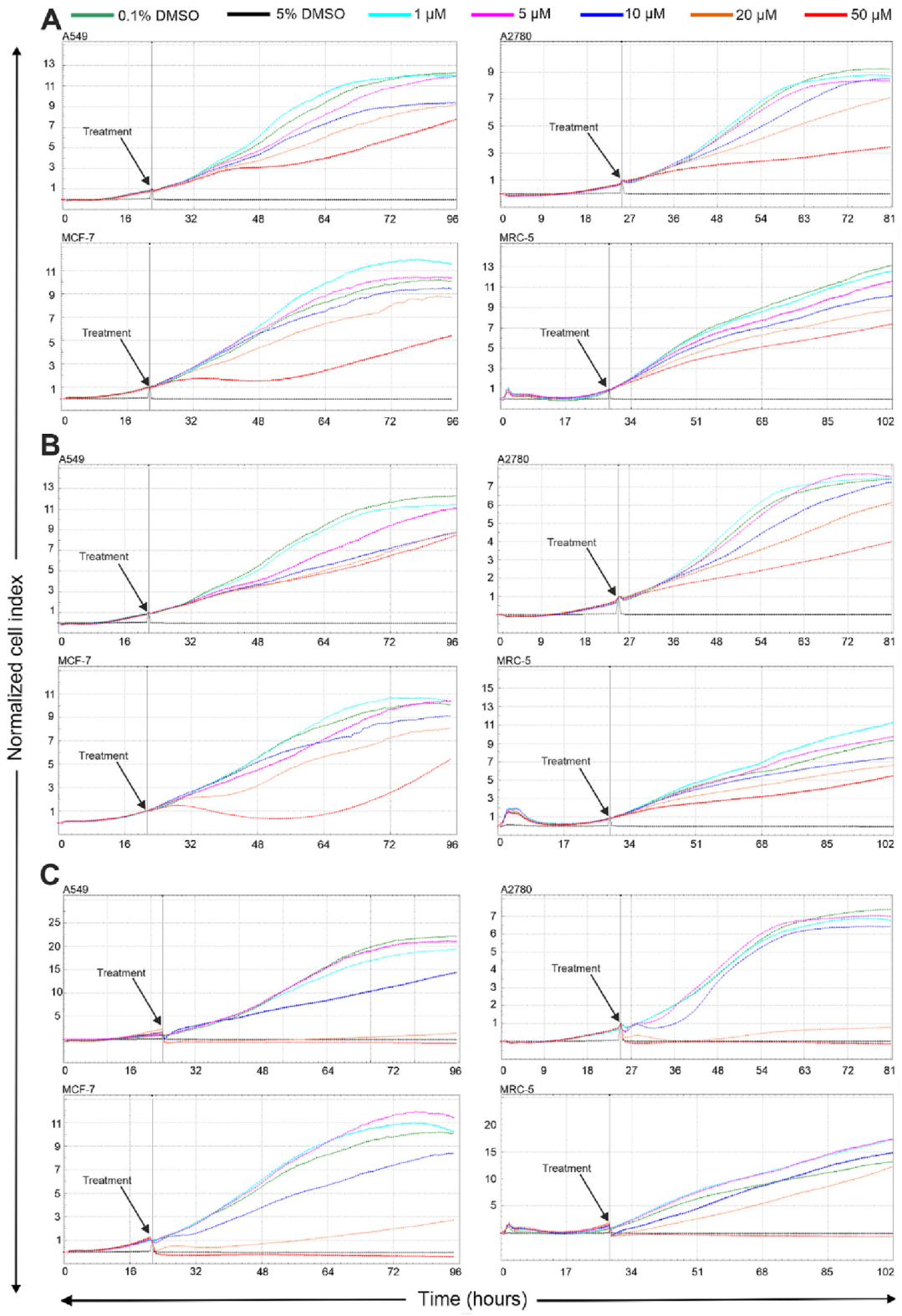

Fig. 5. The effect of derivatives **10** (A), **16** (B), and **32** (C) during 72 h exposure on the proliferation of A549, A2780, MCF-7, and MRC-5 cells was measured by normalized cell index in the xCELLigence system. Control cells were treated with 0.1% DMSO (negative control) and 5% DMSO (positive control). Results of one representative experiment (from three independent experiments) are shown.

(3.7 μg/mL), melanoma MEL-2 (3.2 μg/mL), squamous cell carcinoma A431 (4.9 μg/mL), prostate carcinoma LNCaP (1.7 μg/mL), breast carcinoma ZR-75–1 (1.8 μg/mL) and murine lymphoid leukemia P388 (0.6 μg/mL). The inactivity (ED_{50} greater than 20 μg/mL) of augustine was observed only in the case of the vinblastine-resistant line of epithelial carcinoma KB (Likhitwitayawuid et al., 1993; Nair et al., 2012; 2016a, 2016b). Exposure to the β-crinane alkaloid ambelline in a single-dose

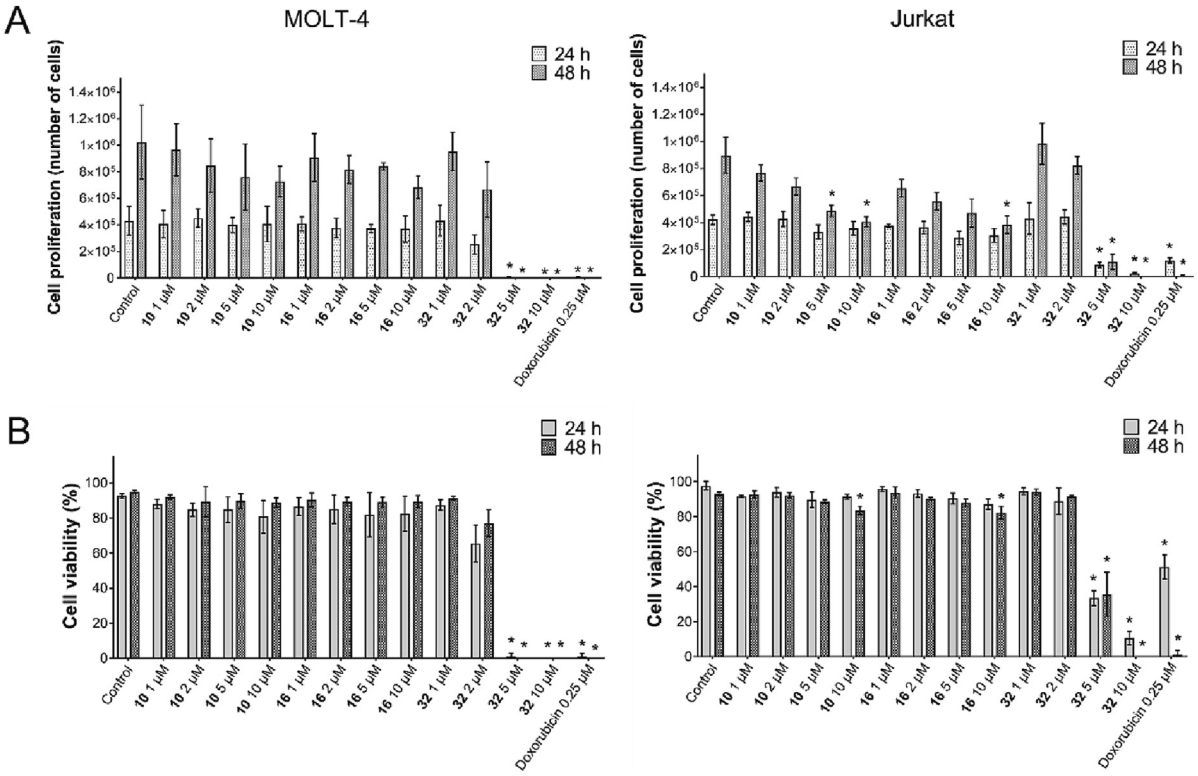

Fig. 6. Proliferation (**A**) and viability (**B**) of MOLT-4 and Jurkat cells after treatment with **10**, **16**, and **32**. Cytostatic and cytotoxic effects of **10**, **16**, and **32** on MOLT-4 and Jurkat cells were quantified by Trypan blue staining method 24 and 48 h after the exposure. Results were obtained with a light microscope and are shown as mean ± SD from three experiments; the * indicates that results are significantly different from the control ($P \leq 0.05$). Cells treated with the conventional cytotoxic agent doxorubicin at 0.25 μM and 0.1% DMSO were used as positive and negative controls, respectively.

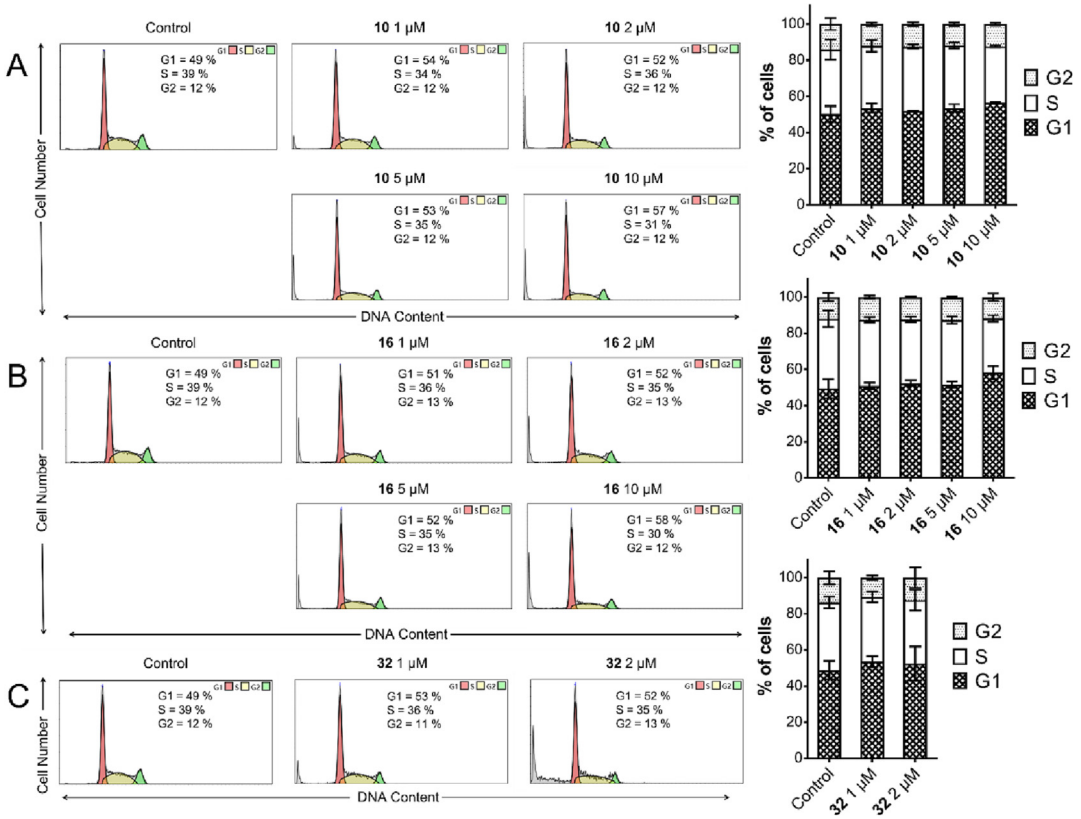

Fig. 7. Cell cycle analysis of different concentrations of **10** (**A**), **16** (**B**), and **32** (**C**) in MOLT-4 cells after treatment for 24 h. The figure depicts flow cytometry results showing distributions of cell populations in the G1, S, and G2 phases. The data are presented as representative of one of three independent flow cytometry histograms, and data analysis is presented as the mean ± SD of three independent experiments. * - indicates the results that are significantly different ($P \leq 0.05$) from the 0.1% DMSO vehicle-treated negative control.

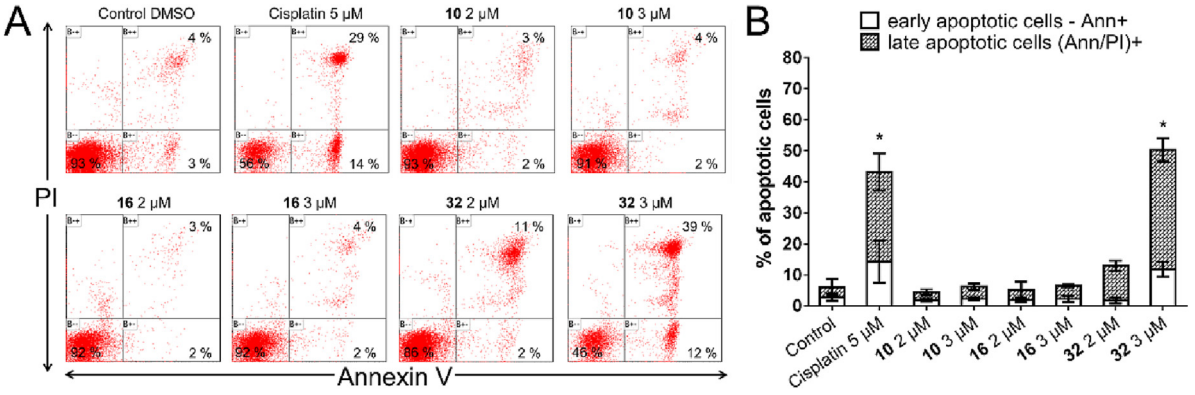

Fig. 8. The quantitative analysis of early and late apoptosis in MOLT-4 cells by flow cytometry after cells were exposed to different concentrations of **10**, **16**, and **32** for 24 h. As a positive control, cisplatin at a 5 μM dose was used. (**A**) Representative histograms were acquired using a CytoFLEX LX flow cytometer and are shown as one of three replicate experiments. (**B**) The bar graph summarizes the mean ± SD percentage of Annexin V-positive (early apoptotic) cells and Annexin V- and PI-double positive (the late phase apoptotic) cells analysed by flow cytometry (n = 3). * Significantly different from the control for early and late apoptotic cells ($P \leq 0.05$).

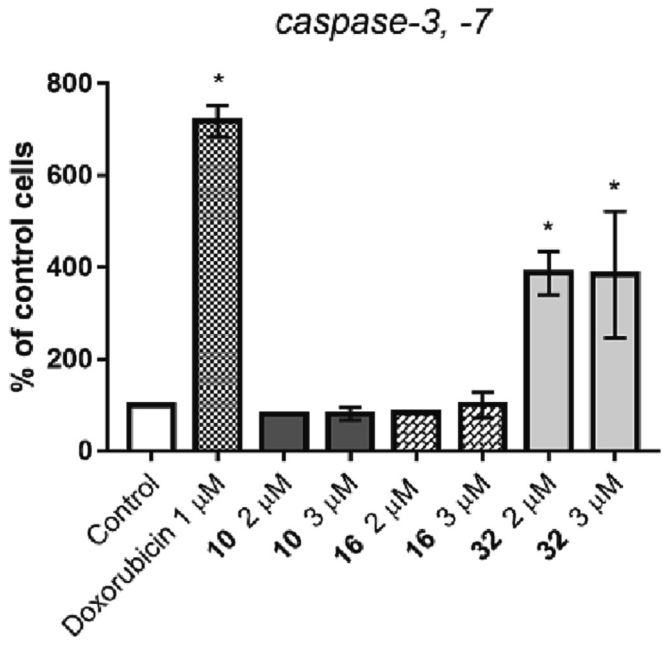

Fig. 9. Detection of caspase-3/-7 activity in MOLT-4 cells after treatment with **10**, **16**, and **32** for 24 h. Data were calculated from at least three independent biological repeats and are expressed as a percent of caspase activity compared to 0.1% DMSO vehicle exposed control cells (100 %). * Significantly different from the control ($P \leq 0.05$). As a positive control, cells treated with conventional chemotherapeutic agent 1 μM doxorubicin were used.

screening concentration of 10 μM induced only a very weak activity capable of negatively affecting the growth and viability of glioblastoma (U373, Hs683) and melanoma (SKMEL) tumour cells (Nair et al., 2012; 2016a, 2016b).

As part of our ongoing efforts to optimize isoquinoline alkaloids as chemotherapeutic agents, the correlation between different substitutions of ambelline derivatives and their cytotoxicity was investigated. An initial single-dose screening was performed on different cancer cell lines of different tissue origins. Thereafter, analysis of cytotoxicity screening data revealed that the greatest antiproliferative activities showed new derivatives from the methylbenzoyl group (**10**), the methoxybenzoyl group (**16** and **17**), and the group of compounds with different disubstitution on the aromatic ring (**32**). The most active ambelline derivatives with an average IC_{50} value below 3 μM for compound **32**, below 4 μM for compound **16**, and 9 μM for compound **10** were further evaluated against MOLT-4 T-lymphoblastic leukemia cells. The Trypan blue staining assay in MOLT-4 cells showed that maximum cell growth-inhibitory activity with a negative impact on cell viability was observed for derivative 32. In addition, we evaluated the effect of ambelline derivatives on cancer cell proliferation using the xCELLigence system. To date, there is only one study investigating the real-time cytotoxicity of the crinane series of Amaryllidaceae alkaloids (Havelek et al., 2017). Havelek and co-workers screened ten crinane-type alkaloids (including ambelline and 11-*O*-acetylambelline) for their antiproliferative activity against human breast adenocarcinoma SK-BR-3 cells using the xCELLigence system. Among these ten crinane-type alkaloids tested, only haemanthamine and haemanthidine (α-crinanes) demonstrated significant antiproliferative activity. Ambelline, 11-*O*-acetylambelline, and other tested β-crinane alkaloids were almost inactive (Vaneckova et al., 2016). Our results are consistent with this study.

Previous studies have investigated the antiproliferative effects of β-crinane alkaloids on a variety of human cancer cell lines (Nair et al., 2012; 2016a, 2016b; Qing et al., 2018). To evaluate how these observations may be related to perturbations in cell-cycle progression, we decided to perform flow cytometric cell cycle analyses. In our study, within 24 h post-treatment administration of ambelline derivatives **10**, **16,** and **32** caused no significant effect on cell cycle progression. The corresponding analogue to derivative **32**, 11-O-(4-chloro-3-nitrobenzoyl)haemanthamine, was studied in more depth to describe the modulation of the cell cycle progression. To rule out a possible hydrolysis product responsible for such activity, the cytotoxicity of 4-chloro-3-nitrobenzoic acid was tested. It did not show any effect under the same conditions as the tested derivative. Uher and co-workers screened 29 derivatives of haemanthamine for their cytotoxic activity. Most analogues contain the same substitution on C-11 of haemanthamine as the ambelline ones presented in this paper, allowing their comparison. Unexpectedly, ambelline derivatives showed a broader scale and higher cytotoxic potential. Only 11-O-(3,5-dinitrobenzoyl) and 11-O-(4-chloro-3-nitrobenzoyl) derivatives of haemanthamine showed better activity than ambelline analogue with mean GP 33 and 5. Haemanthamine, unlike ambelline, is known for its cytotoxic activity, but most of the synthesized derivatives lost the natural cytotoxic potential of haemanthamine. On the other hand, ambelline derivatization was beneficial, providing an enhancement in activity (Uher et al., 2022).

Indeed, apoptosis is an integral part of cytotoxicity and is the preferred mode of cell death induced by anticancer agents. Its typical biochemical markers distinguish it from other types of cell

death (Baig et al., 2016). The notable increase in the total percentage of apoptotic cells and activation of caspase-3/-7, as determined through Annexin V/PI staining and Caspase-Glo 3/7 assay, are quantitative biochemical markers of apoptosis. Our Annexin V/PI staining results revealed that derivative **32** administrated at 3 μM resulted in a significant increase in apoptotic cell populations. To further confirm findings on the apoptosis-inducing effect, we tested whether ambelline analogues **10**, **16,** and **32** affected the activity of caspase-3/-7. In line with the flow cytometric approaches to apoptosis detection, exposure of MOLT-4 cells with **32** at 2 μM and 3 μM for 24 h led to an increase in executive caspase-3/-7 activity. Similar to **32**, some other semisynthetic alkaloid derivatives from the Amaryllidaceae family, such as lycorine analogues (McNulty et al., 2009) and pancratistatin analogues (Ma et al., 2017), were found to exert their cytotoxic activity via apoptosis activation.

5. Conclusions

In the present study, a mini-library of ambelline derivatives was prepared and subjected to 10 μM single-dose cytotoxic screening. Four derivatives (**8, 27**–**29**) selectively inhibited the proliferation of Jurkat acute T-cell leukemia cells. But 11-*O*-benzoylambelline substituted at the benzoyl moiety with methyl (**10**), methoxy (**12**–**17**), ethoxy (**18**), and 4-chloro-3-nitro (**32**) groups showed the highest cytotoxic response after treatment, and the lowest IC_{50} values, even against resistant tumour cell lines, such as PANC-1. In fact, among these selected compounds, **32** exhibited great antiproliferative potency in a dose- and time-dependent manner. In addition, this derivative showed considerable cytotoxicity towards MOLT-4 cells by causing decreased viability and inducing apoptotic cell death. For good measure, effects of **32** were compared with the results of its structural relative derived from haemanthamine, showing a slightly lower cytotoxic potential than 11-*O*-(4-chloro-3-nitro)haemanthamine. This finding could describe how the primary structure of different alkaloid types with the same aromatic moiety on C-11 affects anticancer activity. Another important conclusion is that the most active selective inhibitors of *h*BuChE (**7**, **11**, **26**), previously reported, are not cytotoxic to the tested panel of cell lines (cancer and non-cancer), which makes them suitable for further investigation.

Declaration of Competing Interest

The authors declare that they have no known competing financial interests or personal relationships that could have appeared to influence the work reported in this paper.

Acknowledgments

The skilful technical assistance of Mrs. Nadezda Mazankova and Mrs. Bozena Janska is greatly acknowledged. The authors are grateful to prof. Gerald Blunden for proof-reading the manuscript. This project was supported by the project: Pre-application research into innovative medicines and medical technologies reg. No. CZ.02.1.01/0.0/0.0/18_069/0010046, co-funded by the European Union. This study was also supported by the Cooperatio Program, research area DIAG, SVV 260 548, SVV-260543, and GA UK Nr. 328121 of Charles University.

Appendix A. Supplementary material

Supplementary data to this article can be found online at https://doi.org/10.1016/j.jsps.2023.06.017.

References

Baig, S., Seevasant, I., Mohamad, J., et al., 2016. Potential of apoptotic pathway-targeted cancer therapeutic research: where do we stand? Cell Death Dis. 7. https://doi.org/10.1038/cddis.2015.275.

Berkov, S., Romani, S., Herrera, M., et al., 2011. Antiproliferative alkaloids from *Crinum zeylanicum*. Phytother Res. 25, 1686–1692. https://doi.org/10.1002/ptr.3468.

Cahlikova, L., Kawano, I., Rezacova, M., et al., 2021. The Amaryllidaceae alkaloids haemanthamine, haemanthidine and their semisynthetic derivatives as potential drugs. Phytochem Rev. 20, 303–323. https://doi.org/10.1007/s11101-020-09675-8.

Campbell, W.E., Nair, J.J., Gammon, D.W., et al., 1998. Cytotoxic and antimalarial alkaloids from *Brunsvigia littoralis*. Planta Med. 64, 91–93. https://doi.org/10.1055/s-2006-957381.

Cao, Z.F., Yang, P., Zhou, Q.S., 2013. Multiple biological functions and pharmacological effects of lycorine. Sci. China Chem. 56, 1382–1391. https://doi.org/10.1007/s11426-013-4967-9.

Choudhari, A.S., Mandave, P.C., Deshpande, M., et al., 2020. Phytochemicals in cancer treatment: from preclinical studies to clinical practice (vol 10, 1614, 2020). Front. Pharmacol. 11. https://doi.org/10.3389/fphar.2020.00175.

Cragg, G.M., Pezzuto, J.M., 2016. Natural products as a vital source for the discovery of cancer chemotherapeutic and chemopreventive agents. Med. Prin. Pract. 25, 41–59. https://doi.org/10.1159/000443404.

Ding, Y., Qu, D., Zhang, K.M., et al., 2017. Phytochemical and biological investigations of Amaryllidaceae alkaloids: a review. J. Asian Nat. Prod. Res. 19, 53–100. https://doi.org/10.1080/10286020.2016.1198332.

Doskocil, I., Hostalkova, A., Safratova, M., et al., 2015. Cytotoxic activities of Amaryllidaceae alkaloids against gastrointestinal cancer cells. Phytochem. Lett. 13, 394–398. https://doi.org/10.1016/j.phytol.2015.08.004.

Ferlay, J., Colombet, M., Soerjomataram, I., et al., 2021. Cancer statistics for the year 2020: an overview. Int. J. Cancer. https://doi.org/10.1002/ijc.33588.

Furst, R., 2016. Narciclasine - an amaryllidaceae alkaloid with potent antitumor and anti-inflammatory properties. Planta Med. 82, 1389–1394. https://doi.org/10.1055/s-0042-115034.

Guichard, N., Guillarme, D., Bonnabry, P., et al., 2017. Antineoplastic drugs and their analysis: a state of the art review. Analyst. 142, 2273–2321. https://doi.org/10.1039/c7an00367f.

Habartova, K., Cahlikova, L., Rezacova, M., et al., 2016. The biological activity of alkaloids from the Amaryllidaceae: from Cholinesterases inhibition to anticancer activity. Nat Prod Commun. 11, 1587–1594. https://doi.org/10.1177/1934578X1601101038.

Hanh, T.T.H., Anh, D.H., Huong, P.T.T., et al., 2018. Crinane, augustamine, and beta-carboline alkaloids from Crinum latifolium. Phytochem Lett. 24, 27–30. https://doi.org/10.1016/j.phytol.2018.01.004.

Havelek, R., Seifrtova, M., Kralovec, K., et al., 2014. The effect of Amaryllidaceae alkaloids haemanthamine and haemanthidine on cell cycle progression and apoptosis in p53-negative human leukemic Jurkat cells. Phytomedicine 21, 479–490. https://doi.org/10.1016/j.phymed.2013.09.005.

Havelek, R., Muthna, D., Tomsik, P., et al., 2017. Anticancer potential of Amaryllidaceae alkaloids evaluated by screening with a panel of human cells, real-time cellular analysis and Ehrlich tumor-bearing mice. Chem-Biol Interact. 275, 121–132. https://doi.org/10.1016/j.cbi.2017.07.018.

He, M.M., Qu, C.R., Gao, O.D., et al., 2015. Biological and pharmacological activities of Amaryllidaceae alkaloids. Rsc Adv. 5, 16562–16574. https://doi.org/10.1039/c4ra14666b.

Likhitwitayawuid, K., Angerhofer, C.K., Chai, H.B., et al., 1993. Traditional Medicinal-Plants of Thailand. 22. Cytotoxic and Antimalarial Alkaloids from the Bulbs of *Crinum amabile*. J. Nat. Prod. 56, 1331–1338. https://doi.org/10.1021/np50098a017.

Luchetti, G., Johnston, R., Mathieu, V., et al., 2012. Bulbispermine: a crinine-type amaryllidaceae alkaloid exhibiting cytostatic activity toward apoptosis-resistant glioma cells. Chemmedchem 7, 815–822. https://doi.org/10.1002/cmdc.201100608.

Ma, D., Pignanelli, C., Tarade, D., et al., 2017. Cancer cell mitochondria targeting by pancratistatin analogs is dependent on functional complex II and III. Sci Rep-Uk. 7, 42957. https://doi.org/10.1038/srep42957.

Marikova, J., Ritomska, A., Korabecny, J., et al., 2020. Aromatic Esters of the crinane amaryllidaceae alkaloid ambelline as selective inhibitors of butyrylcholinesterase. J. Nat. Prod. 83, 1359–1367. https://doi.org/10.1021/acs.jnatprod.9b00561.

Masi, M., Di Lecce, R., Merindol, N., et al., 2022. Cytotoxicity and antiviral properties of alkaloids isolated from *Pancratium maritimum*. Toxins. 14 (4), 262. https://doi.org/10.3390/toxins14040262.

McNulty, J., Nair, J.J., Codina, C., et al., 2007. Selective apoptosis-inducing activity of crinum-type Amaryllidaceae alkaloids. Phytochemistry. 68, 1068–1074. https://doi.org/10.1016/j.phytochem.2007.01.006.

McNulty, J., Nair, J.J., Bastida, J., et al., 2009. Structure-activity studies on the lycorine pharmacophore: a potent inducer of apoptosis in human leukemia cells. Phytochemistry. 70, 913–919. https://doi.org/10.1016/j.phytochem.2009.04.012.

Nair, J.J., Bastida, J., Codina, C., et al., 2013a. Alkaloids of the South African Amaryllidaceae: a review. Nat Prod Commun. 8, 1335–1350. https://doi.org/10.1177/1934578X1300800938.

Nair, J.J., van Staden, J., 2019. The Amaryllidaceae as a source of antiplasmodial crinane alkaloid constituents. Fitoterapia. 134, 305–313. https://doi.org/10.1016/j.fitote.2019.02.009.

Nair, J.J., Bastida, J., Viladomat, F., et al., 2012. Cytotoxic agents of the crinane series of Amaryllidaceae alkaloids. Nat. Prod. Commun. 7, 1677–1688. https://doi.org/10.1177/1934578X1200701234.

Nair, J.J., Bastida, J., Viladomat, F., et al., 2013b. Cytotoxic agents of the crinane series of Amaryllidaceae alkaloids. Nat. Prod. Commun. 8, 553–564. https://doi.org/10.1177/1934578X1200701234.

Nair, J.J., Rarova, L., Strnad, M., et al., 2013c. Alkaloids from *Boophone haemanthoides* (Amaryllidaceae). Nat. Prod. Commun. 8, 1705–1710. https://doi.org/10.1177/1934578X1300801211.

Nair, J.J., Rarova, L., Strnad, M., et al., 2014. Crinane alkaloids of the Amaryllidaceae with cytotoxic effects in human cervical adenocarcinoma (HeLa) cells. Nat. Prod. Commun. 9, 461–466. https://doi.org/10.1177/1934578X1400900406.

Nair, J.J., Rarova, L., Strnad, M., et al., 2015. Mechanistic insights to the cytotoxicity of Amaryllidaceae alkaloids. Nat. Prod. Commun. 10, 171–182. https://doi.org/10.1177/1934578X1501000138.

Nair, J.J., Bastida, J., van Staden, J., 2016a. *In vivo* cytotoxicity studies of Amaryllidaceae alkaloids. Nat. Prod. Commun. 11, 121–132. https://doi.org/10.1177/1934578X1601100134.

Nair, J.J., van Staden, J., 2014. Cytotoxicity studies of lycorine alkaloids of the Amaryllidaceae. Nat. Prod. Commun. 9, 1193–1210. https://doi.org/10.1177/1934578X1400900834.

Nair, J.J., Van Staden, J., Bastida, J., 2016b. Cytotoxic alkaloid constituents of the Amaryllidaceae. Stud. Natural Products Chem. 49, 107–156. https://doi.org/10.1016/B978-0-444-63601-0.00003-X.

Pellegrino, S., Meyer, M., Zorbas, C., et al., 2018. The Amaryllidaceae alkaloid haemanthamine binds the eukaryotic ribosome to repress cancer cell growth. Structure 26, 416–425. https://doi.org/10.1016/j.str.2018.01.009.

Qing, Z.X., Huang, J.L., Yang, X.Y., et al., 2018. Anticancer and reversing multidrug resistance activities of natural isoquinoline alkaloids and their structure-activity relationship. Curr. Med. Chem. 25, 5088–5114. https://doi.org/10.2174/0929867324666170920125135.

Seifrtova, M., Havelek, R., Cahlikova, L., et al., 2017. Haemanthamine alters sodium butyrate-induced histone acetylation, p21(WAF1/Cip1) expression, Chk1 and Chk2 activation and leads to increased growth inhibition and death in A2780 ovarian cancer cells. Phytomedicine 35, 1–10. https://doi.org/10.1016/j.phymed.2017.08.019.

Uher, M., Hroch, M., Perinova, R., et al., 2022. Semisynthetic derivatives of haemanthamine and their *in vitro* antiproliferative activity evaluation against a panel of human cell lines. Arabian J. Chem. 15,. https://doi.org/10.1016/j.arabjc.2022.103746 103746.

Vaneckova, N., Hostalkova, A., Safratova, M., et al., 2016. Isolation of Amaryllidaceae alkaloids from *Nerine bowdenii* W. Watson and their biological activities. Rsc Adv. 6, 80114–80120. https://doi.org/10.1039/c6ra20205e.

Youssef, D.T.A., Shaala, L.A., Altyar, A.E., 2022. Cytotoxic phenylpropanoid derivatives and alkaloids from the flowers of Pancratium maritimum L. Plants (Basel). 11. https://doi.org/10.3390/plants11040476.